

**Synthesis, Structure-Activity Relationships, Molecular Modelling and Cytotoxicity of 2-Aryl-1,4-Naphthoquinone-1-Oxime Methyl Ethers through Inhibiting Tubulin Polymerization.**

A thesis submitted to the

**Chiba University**

In fulfillment of the requirements of the

**Degree of Doctor of Philosophy**



By

**Scebi J. Mkhize**

Department of Pharmaceutical Sciences

Chiba University

Inohana, 1-8-1

Chiba

September 2014

## Acknowledgements

*Dedicated to W. S. Mkhize-Furukawa and Y. Furukawa*

To My Family: Ngicela ukubonga inkosazana yami u-Welile Sarah Mkhize kanje nomama wayo u- Yasuko Furukawa ngosulu lwethu lukuba umndeni. Lomsebenzi ngiwenzele nina bogubhela, bakaMavovo. Ngicela ukuthatha ithuba ngibonge u-Eudy mabuza ngokungiceda ngesikhathi ngihambe esithunzini sikasathane.

I also like to thank the staff of Chiba University and all those who too part in making this thesis a success. Not to forget Dr Masato Takahashi for his great friendship, you were the best.

Kusha mina umashananandana, inkuzi ethenwamasende, yakhula yabayinxaha. Nimbuze kubafana baseNjomelwane, ixhaha elingenambondo elikhuzimpi layilwa layiqeda, kudwa msukele usuyozwa ngobezizwe bethi `kuodwa ubulingwe yini.

Scebi Mkhize

“Invictus”

## **ABSTRACT**

This thesis concerns the synthesis and biological evaluation of microtubules (MT) inhibitors of the type 2-aryl-1,4-naphthoquinone-1-oxime methyl ether.

Following a comprehensive review on MT and MT targeting drugs, the first part of the Results and Discussion section (Chapter 2) of the thesis, a library of derivatives of 2-aryl-substituted (Chapter 3) are described and evaluated for their inhibitory activity against tubulin in HeLa cell culture.

## ABBREVIATIONS

AcOH	Acetic acid
aq.	Aqueous
Ar	Aromatic
BnBr	Benzyl bromide
Boc	<i>tert</i> -Butyl carbonate
BOP	Benzotriazol-1-yloxy-tris(dimethylamino) Phosphonium hexafluoro phosphate
br	Broad
brs	Broad singlet
cat.	Catalytic
CF <sub>3</sub> SO <sub>3</sub> H(TfOH)	Trifluoromethanesulfonic acid
CH <sub>2</sub> Cl <sub>2</sub>	Dichloromethane / Methylene chloride
CH <sub>3</sub> CN	Acetonitrile
δ	Chemical shift in ppm
d	Doublet
dd	Doublet of doublets
dt	Doublet of triplets
DBU	1,8-Diazabicyclo[5.4.0]undec-7-ene
DCC	1,3-Dicyclohexylcarbodiimide
DCM	Dichloromethane / Methylene chloride
DMAP	<i>N,N</i> -Dimethylaminopyridine
DMSO	Dimethylsulfoxide
ES	Electron spray
Et <sub>3</sub> N	Triethylamine
Et <sub>2</sub> O	Diethyl ether
EtOAc	Ethyl acetate
EtOH	Ethanol
eq.	Equivalent
FAB	Fast atom bombardment
g	Grams
HCl	Hydrochloric acid
HPLC	High-pressure liquid chromatography
hr.	Hour

HRMS	High-resolution mass spectrometry
Hz	Hertz
IR	Infrared spectrometry
<i>J</i>	Coupling constant
Lit.	Literature
<i>m</i>	Meta
m	Multiplet
M <sup>+</sup>	Molecular ion
MeOH	Methanol
mg	Milligram(s)
MHz	Mega hertz
ml	Millilitre(s)
mmol	Millimole(s)
Mp	Melting point
MsCl	Methanesulfonyl chloride
<i>m/z</i>	Mass to charge ratio
NBS	<i>N</i> -Bromosuccinamide
NMR	Nuclear magnetic resonance
NRTI	Nucleoside reverse transcriptase inhibitor
<i>o</i>	Ortho
<i>p</i>	Para
PG	Protecting group
P(OEt) <sub>3</sub>	Triethyl phosphite
Pd/C	Palladium-on-carbon
Pet ether	Petroleum ether
PPh <sub>3</sub>	Triphenylphosphine
(PPh <sub>3</sub> ) <sub>4</sub> P	Tetrakis(triphenylphosphine)palladium (0)
rt	Room temperature
s	Singlet
t	Triplet
TBDMSCl	<i>tert</i> -Butyldimethylsilyl chloride
TBDPS	<i>tert</i> -Butyldiphenylsilyl chloride
td	Triplet of doublets
TFA	Trifluoroacetic acid
THF	Tetrahydrofuran
TLC	Thin layer chromatography

TMSCl	Trimethylsilyl chloride
<i>p</i> -TsOH	<i>para</i> -Toluenesulfonic acid
q	Quartet
UV	Ultra violet
w/v	Weight by volume
v/v	Volume by volume

# Synthesis, Structure-Activity Relationships, Molecular Modelling and Cytotoxicity of 2-Aryl-1,4-Naphthoquinone-1-Oxime Methyl Ethers through Inhibiting Tubulin Polymerization.

## Chapter 1

### Introduction

According to world health organisation's (WHO), International Agency for Research on Cancer (IARC) figures, cancer is the leading cause of death worldwide, accounting for 8.2 million death in 2012.<sup>1</sup> Cancer is a generic term for a large group of disease that can affect any part of the body. It results from unique and unpredictable alteration of the genome on the cell. The cancerous genome may contain a number of points of mutations, translocations, fusions and other aberrations. The cancerous cell then rapidly create other abnormal cells which grows beyond their boundaries and invade adjoining parts of the body and spread to other organs, referred to as metastasis.

Since the emergence of cancer, radiotherapy relatively remained a major modality of cancer therapy. Theoretically, radiotherapy uses high-energy X-ray or (rarely)  $\gamma$ -ray radiation to kill cancer cells by directly damaging DNA structure or by creating charged particles (free radicals) within the cells that can in turn break down the DNA. Over the decades, radiotherapy experienced great improvement and a sufficient dose can render any tumor cell harmless, improvements have included the use of megavolts ( 6-25 MV) X-rays to avoid skin damage, Intensity-modulated radiation therapy (IMRT) to better concentrate the dose within the shape of the tumor. But despite these advances, radio therapy, mostly, still fail to eradicate tumors, mainly due to emergence of hypoxic tumors, potential radio-toxicity to normal cells, and the end-results of cumulative damage to normal cells, which in turn become cancerous.

In recent years, chemotherapy has emerged as a generally accepted modality in combating the disease. In chemotherapy, the underlying principle of the approach is to kill the cancer by treating it with chemicals that interfere with vulnerable processes surrounding cell division. Current chemotherapy regimes do this by disrupting microtubule assembly dynamics during mitosis which lead to cell arrest by mitotic check point complex, and eventually promoting apoptosis.<sup>2-4</sup>

Microtubules are filamentous polymers that form one of the major components of the cytoskeletal elements of all eukaryotic cells, that are necessary for many functions, including intracellular transport, motility, morphogenesis and cell division.<sup>5</sup> They are dynamic, ever-changing structures, which mean their ends are alternating between shortening and growth in a process called polymerization, creating a multiplicity of cell shapes in different tissue types. They can dramatically

and rapidly depolymerize and arrange in a single cell to form the mitotic spindle fibres that aligns and separates the chromosomes and can also thereby forming roadways for the transport of cellular cargo and are involved in intracellular signalling.<sup>2</sup> They composed of alpha( $\alpha$ )-tubulin and beta( $\beta$ )-tubulin heterodimers arranged in the form of slender filamentous tubes arranged head-to-tail, of several micrometres long.<sup>6</sup>

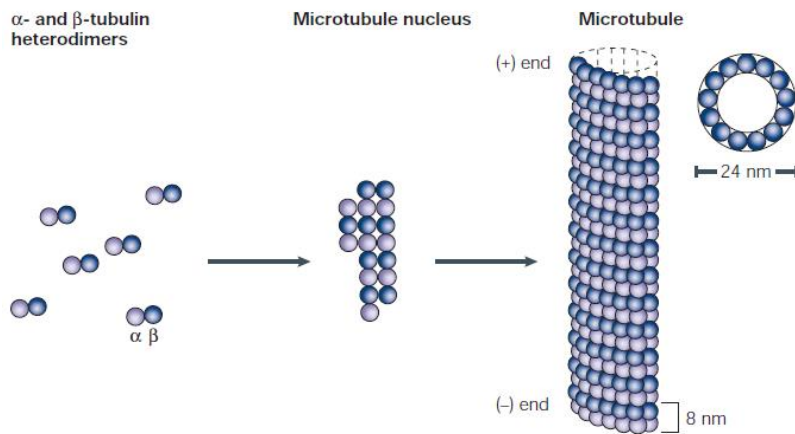


Figure 1.1: Polymerization of microtubules. Heterdimers of  $\alpha$ - and  $\beta$ -tubulin assemble to form a short microtubule nucleus, then elongation.

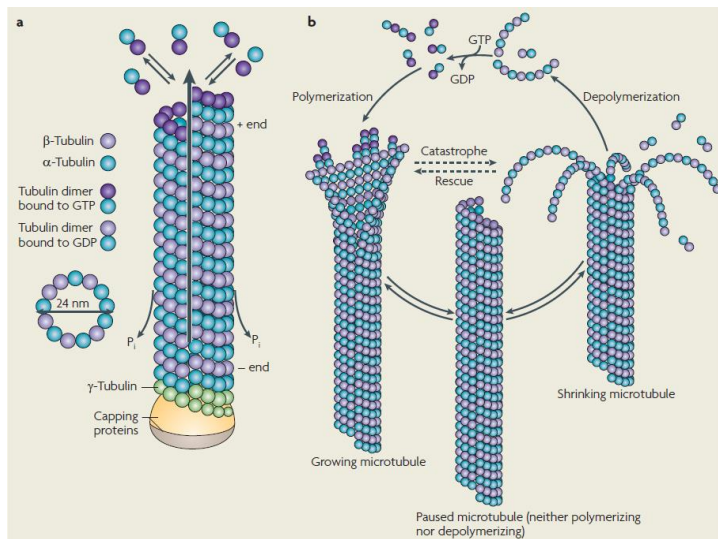


Figure 1.2: Characteristics properties of MT dynamics

The polymerization of microtubules occurs by a mechanism in which relatively slow formation of a short microtubule “nucleus” is followed by rapid elongation of the microtubule as its ends by the reversible, non-covalent addition of tubulin dimers. The  $\alpha$ -tubulin subunit is always bound to GTP, acquiring a conformation suitable for MT polymerization, whereas the  $\beta$ -tubulin subunit can be bound either to GTP or GDP, favorable for MT polymerization or depolymerization, respectively<sup>7</sup>. Then, two ends with different dynamic properties can be distinguished within a MT: the (+)end, which is terminated by  $\beta$  subunits, being more dynamic than the (-) end, which is terminated by  $\alpha$

subunits. The dynamic instability model of MT assembly was proposed by Mitchison and Kirschner in 1984<sup>8</sup>. They proposed that individual MTs exist either in an elongation state or a rapidly shortening state, with abrupt and apparently random transitions between these two states. MTs are thus governed by an intrinsic property involving repetitive spurts of shortening from their plus ends, followed by periods of polymerization. This non-equilibrium behavior is based on the binding and hydrolysis of GTP at the nucleotide exchangeable site (E-site) in  $\beta$  tubulin. Only dimers that have GTP in their E-site can polymerize. This nucleotide is then hydrolyzed and becomes non-exchangeable. The GTP cap model proposes that the GDP-tubulin core of MT is stabilized at the plus end by a layer of GTP-tubulin subunits that may act to maintain association between protofilaments<sup>9</sup>. When this cap is stochastically lost, the protofilaments peel outward and the MT rapidly depolymerizes. Although both MT ends can either grow or shorten, the changes in length at the plus end are much greater than at the minus end. Thus, there are four variable characteristics of dynamic instability<sup>7,10</sup>: the rate of microtubule growth; the rate of shortening; the frequency of transition from the growth or paused state to shortening (this transition is called a ‘catastrophe’); and the frequency of transition from shortening to growth or pause (called a ‘rescue’). Pause is defined as a period when changes in microtubule length are undetectable by light microscopy and Dynamicity is a combination parameter, describes the overall detectable rate of exchange of tubulin dimers with microtubule ends. The second dynamic behavior, called ‘treadmilling’, is net growth at one microtubule end and balanced net shortening at the opposite end. It involves the intrinsic flow of tubulin subunits from the plus end of the microtubule to the minus end and is created by differences in the critical subunit concentrations at the opposite microtubule ends. (The critical subunit concentrations are the concentrations of free tubulin subunits in equilibrium with the microtubule ends.) This behavior occurs in cells as well as *in vitro*, and might be particularly important in mitosis<sup>11</sup>. Treadmilling and dynamic instability are compatible behaviors, and a specific microtubule population can show primarily treadmilling behavior, dynamic-instability behavior or some mixture of both<sup>12</sup>.

Microtubules are exquisitely regulated by myriad of mechanisms, differentially both in different “regions” of a cell (e.g. during migration or mitosis). In other words, MT dynamics are regulated both spatially and temporally<sup>13</sup>. Among the mechanisms that can regulate dynamics are tubulin isotype expression, post-translational modification of tubulin, microtubule-associated proteins and microtubule-interacting proteins. With regard to tubulin isotypes, there are at least 6  $\alpha$ -tubulin and 7- $\beta$  tubulin human tubulin isotypes, which are expressed to varying degrees in different cells and tissues<sup>14</sup>. Post-translation modifications include polyglutamylation, polyglycylation, phosphorylation, acetylation, detrosination/trosination, and removal of the penultimate glutamic acid<sup>14,15</sup>. MTs interact with an impressive number of binding proteins, and cellular MT dynamics are thus the result

of the combined effect of stabilizing and destabilizing factors. Regulation can occur at many levels, some proteins regulating tubulin folding, some stabilizing existing MTs such as structural microtubules associated proteins (MAPs), and some interacting with MT ends to influence their dynamics, location and lifespan. The main MT-related proteins that regulate MT dynamics are presented in Table 1<sup>13</sup>.

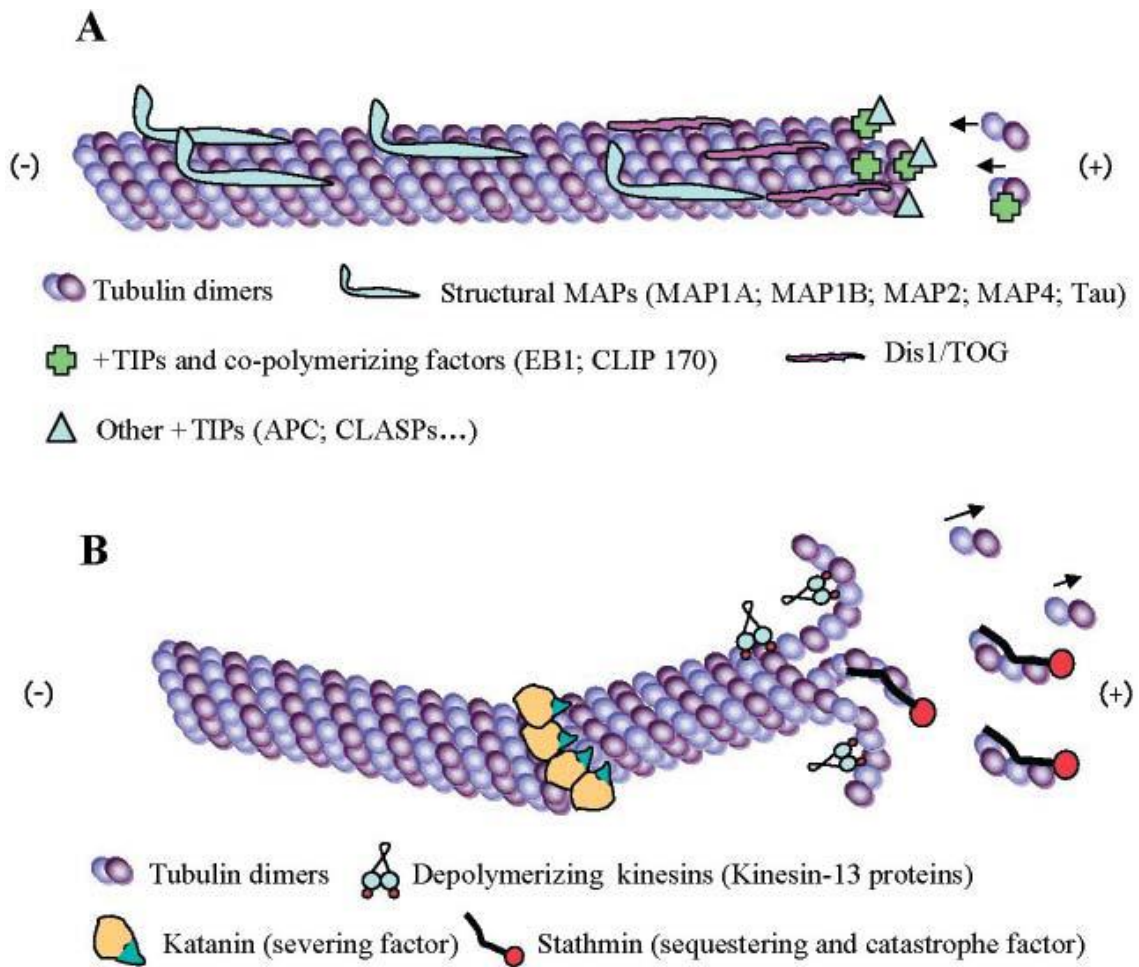


Figure 1.3: MT interaction with the major MT-related proteins. (A) A growing MT and various interactions with stabilizing factors. (B) A shortening MT and various interactions with destabilizing factors. (-) and (+) indicate the minus and the plus ends of the MT, respectively.

#### Microtubule dynamics and oncology

Microtubule dynamics is the principal target in oncology<sup>2,7,16</sup>. This is mainly because microtubules play a critical role in cell division and during mitosis the microtubule dynamics dramatically increase during this phase. At the onset on mitosis, the interphase microtubule network disassembles and is replaced by a new population of spindle microtubules, that is many-fold more

dynamic than the former<sup>17</sup>. It been also noted that during this phase, MAP4, which binds on the surface of microtubules and appears to stabilise microtubule dynamics, after being phosphorylated by cyclin B-cdc2 kinase, results in MAP4 less association with microtubules, which likely contribute to increased MT dynamics. Furthermore, nuclear envelop breakdown releases Ran, a Ras-like GTPase and it chromatin-bound nucleotide-exchange factor (RCC1) which also appear to regulate MT dynamics<sup>18</sup>. Presence of RCC1 probably mediates local high concentration of Ran-GTP, which in turn increase MT dynamics by increased catastrophe and reduced rescue frequencies. This results in accumulation of very dynamics microtubules with bipolar spindle fibres in the region of the chromosomes<sup>19</sup>.

During prophase, microtubules emanate from each of the centromeres at each pole, undergoing rapid catastrophe and rescue, essentially probing the cytoplasm for attachment to the kinetochore<sup>20</sup>. Once they “find” and attachment to kinetochore is achieved, it is essential that microtubules of the opposite pole are dynamic enough to successfully attach to sister kinetochore, resulting in a bipolar spindle. Once achieved, chromosomes gradually congress to the metaphase. Many microtubule-targeted drugs act at this stage to prevent formation of a complete bipolar spindle, as dynamic MTs are crucial to passage to anaphase<sup>21</sup>.

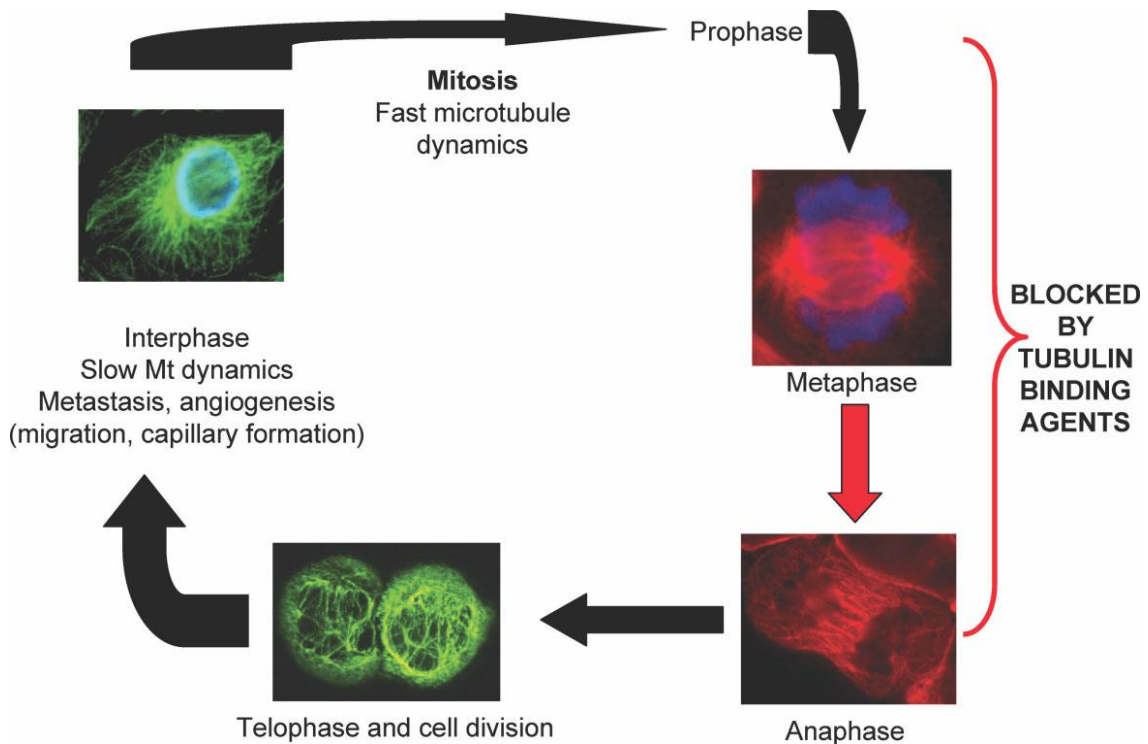


Figure 1.4: Microtubule structures through the cell cycle. Metaphase and anaphase MTs (red), Telophase and interphase MTs (green), Chromosomal DNA (blue).

The spindle checkpoint ensures accurate chromosome segregation in mitosis and meiosis. The

presence of a single chromosome that is unable to achieve a bipolar attachment to the spindle or if there is insufficient tension on kinetochores is sufficient to prevent a cell from transitioning to anaphase; the checkpoint blocks the activity of the anaphase-promoting complex. Upon checkpoint activation, a checkpoint protein complex containing BubR1, Bub3, Mad2 and Cdc20 binds to the anaphase promoting complex, inhibiting its ubiquitin ligase activity, thus the cell then remains blocked in a pro-metaphase/metaphase-like state and eventually undergoes apoptosis. The suppression of microtubules dynamics is the principal mechanism of microtubule-targeted drugs<sup>3,4,22</sup>.

Microtubule-targeted antimitotic drugs are usually classified into two main groups. One group, known as the microtubule-destabilizing agents, inhibits microtubule polymerization at high concentrations and includes several compounds — such as the *Vinca* alkaloids (vinblastine, vincristine, vinorelbine, vindesine and vinflunine), cryptophycins, halichondrins, estramustine, colchicine and combretastatins. The second main group is known as the microtubule-stabilizing agents<sup>23</sup>. These agents stimulate microtubule polymerization and include paclitaxel (the first agent to be identified in this class), docetaxel (Taxotere), the epothilones, discodermolide, the eleutherobins,

Table 1 | **Antimitotic drugs, their diverse binding sites on tubulin and their stages of clinical development**

Binding domain	Related drugs or analogues	Therapeutic uses	Stage of clinical development
Vinca domain	Vinblastine (Velban)	Hodgkin's disease, testicular germ-cell cancer	In clinical use; 22 combination trials in progress
	Vincristine (Oncovin)	Leukaemia, lymphomas	In clinical use; 108 combination trials in progress
	Vinorelbine (Navelbine)	Solid tumours, lymphomas, lung cancer	In clinical use; 29 Phase I-III clinical trials in progress (single and combination)
	Vinflunine	Bladder, non-small-cell lung cancer, breast cancer	Phase III
	Cryptophycin 52	Solid tumours	Phase III finished
	Halichondrins (such as E7389)	–	Phase I
	Dolastatins (such as TZT-1027)	Potential vascular-targeting agent	Phase I; Phase II completed
	Hemiasterlins (such as HTI-286)	–	Phase I
Colchicine domain	Colchicine	Non-neoplastic diseases (gout, familial Mediterranean fever)	Appears to have failed trials, presumably because of toxicity
	Combretastatins (AVE8062A, CA-1-P, CA-4-P, N-acetylcolchicinol-O-phosphate, ZD6126)	Potential vascular-targeting agent	Phase I, II
	2-Methoxyestradiol	–	Phase I
	Methoxybenzene-sulphonamide (such as ABT-751, E7010)	Solid tumours	Phase I, II
Taxane site	Paclitaxel (Taxol), TL00139 and other analogues of paclitaxel	Ovarian, breast and lung tumours, Kaposi's sarcoma; trials with numerous other tumours	In clinical use; 207 Phase I-III trials in the United States; TL00139 is in Phase I trials
	Docetaxel (Taxotere)	Prostate, brain and lung tumours	8 trials in the United States (Phases I-III)
	Epothilones (such as BMS-247550, epothilones B and D)	Paclitaxel-resistant tumours	Phases I-III
	Discodermolide	–	Phase I
Other microtubule binding sites	Estramustine	Prostate	Phases I-III, in numerous combinations with taxanes, epothilones and <i>Vinca</i> alkaloids

sarcodictyins, laulimalide, rhazinalam, and certain steroids and polyisoprenyl benzophenones<sup>24,25</sup>. This classification is based on that microtubule-targeted drugs increase or decrease microtubule polymerization at high concentrations powerfully suppress microtubule dynamics at 10–100-fold, therefore, kinetically stabilize the microtubules, without changing the microtubule-polymer mass. This discovery is contract to the previously held thought that the effects of the two classes of drugs on microtubule polymer mass were the most important actions responsible for their chemotherapeutic properties. The current held dogma is that these drugs suppression of spindle-microtubule dynamics, which results in the slowing or blocking of mitosis at the metaphase–anaphase transition and induction of apoptotic cell death<sup>26,27</sup>.

#### Mechanisms of microtubule-targeted drugs

The *Vinca* alkaloids (vinblastine and vincristine) were isolated from the leaves of the periwinkle plant *Catharanthus roseus* (L.) G. Don.<sup>28</sup> The leaves of the periwinkle plant have been used for their medicinal properties since the seventeenth century. These drugs have been found to depolymerize microtubules and destroy mitotic spindles at high concentrations in Hela cells, thus blocking mitosis

in the dividing cell with condensed chromosomes. While at low, but within clinical concentrations, they were found to suppress microtubule dynamics rather than microtubule polymerization<sup>27</sup>.

The clinically approved vinblastine binds to tubulin and also directly to microtubules, in the  $\beta$ -subunit of tubulin dimers at a distinct region referred as *Vinca* binding domain. Vinblastine binds rapidly and reversibly to tubulin and induces conformational change in tubulin which increases its binding affinity to tubulin. This ability is thought to play a key role in the ability of the drug to stabilize microtubules kinetically<sup>29</sup>.

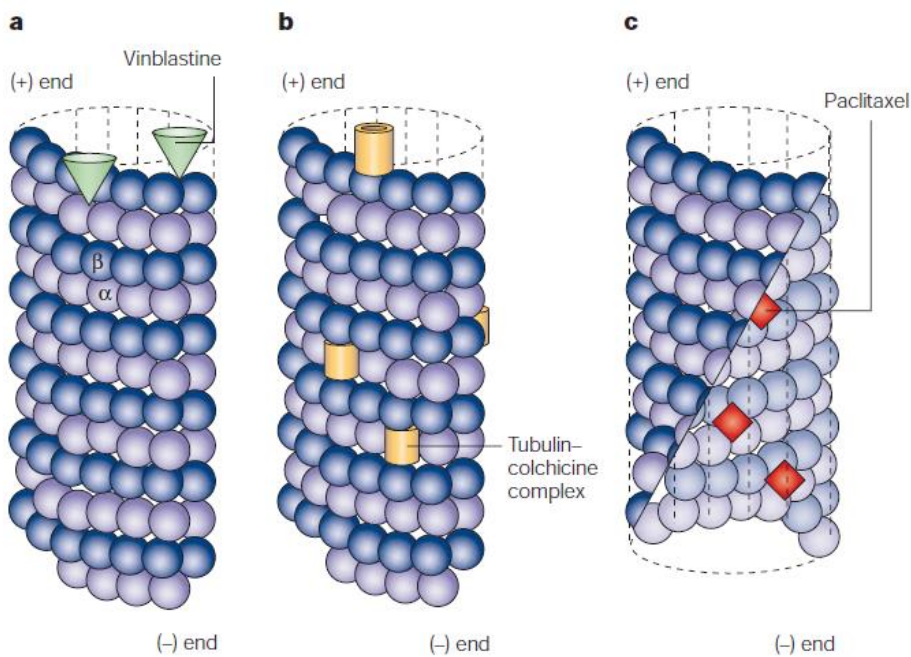


Figure 1.5. Antimitotic drugs bind to microtubules at diverse sites. **a** A few molecules of vinblastine bound to high-affinity sites at the microtubule plus end suffice to suppress microtubule dynamics. **b** Colchicine forms complexes with tubulin dimers and copolymerizes into the microtubule lattice, suppressing microtubule dynamics. **c** A microtubule cut away to show the interior surface is shown. Paclitaxel binds along the interior surface of the microtubule, suppressing its dynamics.

#### Paclitaxel and related drugs

On the other, taxol binds poorly to soluble/ non-polymerized tubulin dimers, but with high affinity to tubulin along the interior length of the microtubule. Binding of paclitaxel to its site on the inside microtubule surface stabilizes the microtubule and increases microtubule polymerization, presumably by inducing a conformational change in the tubulin that<sup>5</sup>, by an unknown mechanism, increases its affinity for neighboring tubulin molecules 24. There is one paclitaxel-binding site on every molecule of tubulin in a microtubule and the ability of paclitaxel to increase microtubule polymerization is associated with nearly 1:1 stoichiometric binding of paclitaxel to tubulin in

microtubules<sup>30</sup>.

### Colchicine

Colchicine is used clinically in the treatment of gout, but including colchicine-related compounds they are not used for the treatment of cancer. This has been said to be attributed by their potent toxicity. Currently several other compounds that bind to the colchicine binding site are under investigation. The interaction of colchicine with tubulin and microtubules presents yet another variation in the mechanisms by which microtubule-active drugs inhibit microtubule function. While it in many ways similar to that of *Vinca* alkaloids, in that colchicine depolymerizes microtubules at high concentrations and stabilizes microtubule dynamics at low concentrations; Colchicine inhibits microtubule polymerization sub-stoichiometrically as oppose to *Vinca* alkaloids (i.e. at concentrations well below the concentration of the tubulin that is free in solution). It is thought that colchicine inhibits microtubule polymerization by binding to microtubule ends rather than to the soluble-tubulin pool. Colchicine probably does not bind to microtubule ends as with *Vinca* alkaloids, rather on soluble tubulin, thereby inducing conformational changes leading to a poorly reversible final state tubulin-colchicine complex. This complex then copolymerizes into the microtubule ends in small numbers along large numbers of free tubulin molecules. While new tubulin addition is not affect, but microtubule dynamics became suppressed. The principle for suppression being that, the incorporated complex should bind more tightly to its neighbors than tubulin itself; hence the rate of catastrophe is reduced (for review, see ref 2 and others within).

Despite differences in the mode of action between *Vinca* colchicine-like drugs and the taxane-like drugs, nearly all of the microtubule-targeted drugs stabilizing microtubule dynamics at their lowest effective concentrations, the suppression/stabilization of microtubule dynamics correlate with blocking of the cell cycle at mitosis and in sensitive tumor cells, ultimately resulting in cell death by apoptosis. Therefore, the most potent mechanism of nearly all of the microtubule-targeted drugs seems to be stabilization of dynamics of mitotic-spindle microtubules<sup>31</sup>.

### Quaternary benzo(c)phenanthridines

Quaternary benzo(c)phenanthridines alkaloids are produced by a number of plant species of the Papaveraceae, Fumariaceae, and Rutaceae families<sup>32</sup>. Herbal extracts from the aforementioned plants have been utilized in folks medicine as antimicrobial, antifungal, and anti-inflammatory agents<sup>33</sup>. They are fully-aromatized alkaloids with an isoquinoline core skeleton and are structurally classified in O<sub>4</sub>-type (R<sup>1</sup>, R<sup>2</sup>, R<sup>3</sup>, R<sup>4</sup> or R<sup>1</sup>, R<sup>2</sup>, R<sup>4</sup>, R<sup>5</sup> = OR), O<sub>5</sub>-type (R<sup>1</sup>, R<sup>2</sup>, R<sup>3</sup>, R<sup>4</sup>, R<sup>6</sup>, R<sup>7</sup> = OR) and O<sub>6</sub>-type (R<sup>1</sup>, R<sup>2</sup>, R<sup>3</sup>, R<sup>4</sup>, R<sup>6</sup>, R<sup>7</sup> = OR) bases dependent upon the number of oxygen functions in their molecules, Figure 1.6<sup>34</sup>. These naturally occurring plant-based alkaloids has displayed an attractive

biological activity as antiproliferation agents<sup>32,35</sup>. Among the O<sub>4</sub>-type, the list include nitidine<sup>36</sup>, NK107<sup>37</sup>, and sanguinarine(SA)<sup>37</sup> chelerythrine (CHE)<sup>32</sup> being the best recognized ones. Macarpine, an antitumor-active O<sub>6</sub>-benzo[*c*]phenanthridine alkaloid has been greatly discussed as potential cytostatic for cancer treatment. Macarpine is only one naturally occurring O<sub>6</sub>-base alkaloid firstly isolated by Slavik et al<sup>38</sup>. In an ongoing research, in Chiba University laboratory by Ishikawa *et al.*<sup>39</sup> they have reported the synthesis of a macarpine using a synthetic strategy base on nitrosation of 1-naphthol followed by the Bischler-Napieralski reaction (BNK) of naphthylformamide. In this study, cytotoxic activity of marcapine (in it chloride form) was tested on HeLa S3 tumor cell and compared to those of the structurally related 2, 3,7, 8, 10-pentaoxygenated (O5) base chlorides, 10-isopropoxysanguinarinel and chelilutine chlorides. Interestingly, marcapine showed the strongest activity among them. On the other hand the least one was observed in chelilutine. In other words additional introduction of a methoxy group into the C2 position of a benzo[*c*]phenanthridine skeleton may cause to enhance the activity, while replacement of a methylenedioxy function at the 7,8 positions by two methoxy groups led to reduction of the activity. These compounds and it intermediates are the subject of this thesis.

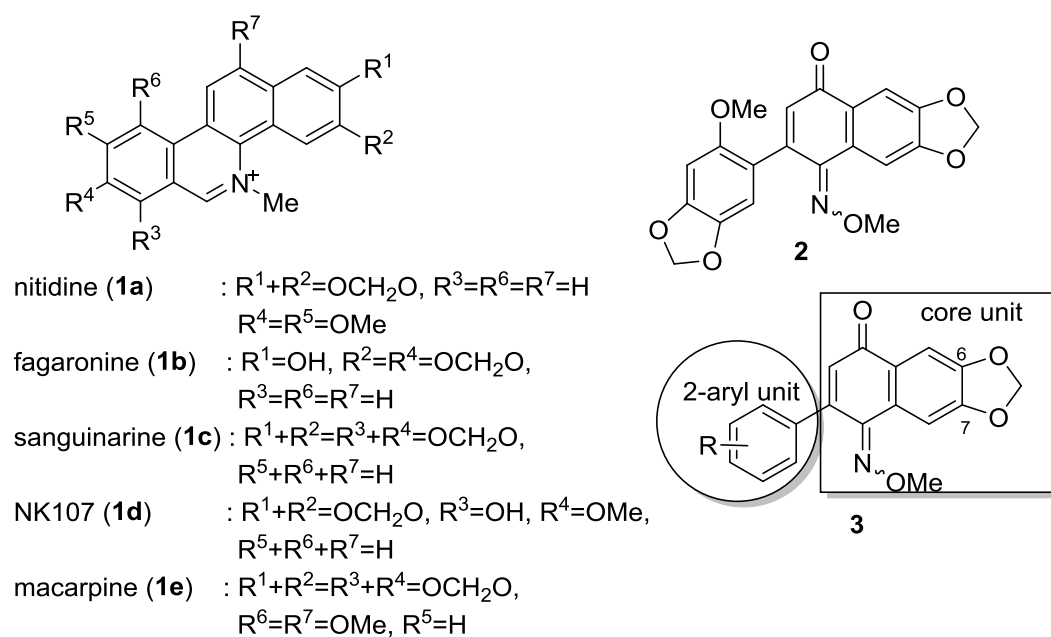


Figure 1.6: Structures of Benzo[*c*]phenanthridine Alkaloids **1a-e**, Naphthoquinone Monooxime ether **2**, and 2-aryl-naphthoquinone-1-oxime methyl ether **3**.

In screening for the discovery of potential anti-tumor active seed compounds, the intermediate QO-1 showed string cytotoxic activity against a number of cell lines. It was also found that **QO-1** induced G2/M-phase arrest in Hela and MCF-7 cells<sup>40</sup>, possibly by inducing microtubule-depolymerization effects similar to that of nocodazole. This was supported by expression of Bub1, one of the spindle

assembly checkpoint (SAC) proteins.

Preliminary experiments on the structure activity-relationship (SAR) of the 6,7-methylenedioxy-1,4-naphthoquinone-1-oxime methyl ether skeleton<sup>34</sup>, a common core structure in the 2-aryl-1,4-naphthoquinone-1-oxime methyl ether derivatives, suggested that it play an important role for the activity of these compounds (see Figure 1.6, structure **3**). In these aforementioned studies, **2** (or **QO-1**) cytotoxicity was evaluated using Hela S3 cell by methylene blue staining method and the IC<sub>50</sub> was estimated to be less than 0.1 ug/ml using Litchfield and Wilcoxon method. Using these results as a positive control for SAR examination, it was found that displacement of the methylenedioxy moieties either in the naphthoquinone skeleton or in the 2-aryl substituent with dimethoxy ones led to reduction of activities. Replacement of both methylene moieties resulted in loss of activity. Furthermore, structural modification of the skeletal core unit of 1,4-naphthoquinone-1-oxime ethers, either the 1,4-naphthoquinone substituents or modification of the oxime moiety, resulted in total loss of activity, hence revealing crucial requirement of the functional 6,7-methylenedioxy-1,4-naphthoquinone-1-oxime methyl ether skeleton in spite of substituent tolerance in the 2-aryl group.

#### Objectives of this thesis

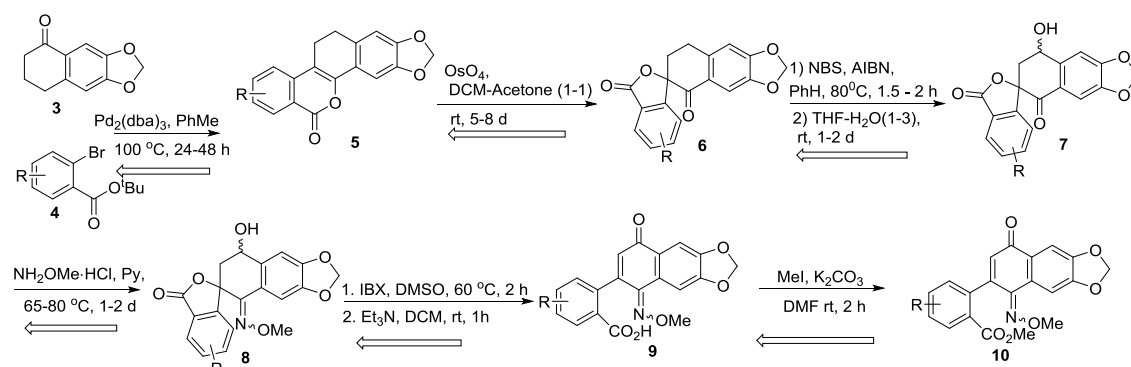
To further explore the SAR and optimize the lead compound **2**, we planned to 1) synthesis 2-aryl-1,4-naphthoquinone-1-oxime methyl ether analogues by modification of the 2-aryl group; 2) biological activity and molecular docking studies of aryl-modified 1,4-naphthoquinone-1-oxime methyl ether.

## Chapter 2

### Results and Discussion

#### Synthetic Plan

The 2-aryl-1,4-naphthoquinone-1-oxime methyl ether compounds were synthesized as outlined in Scheme 2.1. First, the phenyl ring was modified into appropriate *tert*-butyl *o*-bromobenzoate **4**, consisting of appropriate ether. In a modified literature procedure<sup>41</sup> we employed Osium oxidation, dihydroarnottin **6** was prepared from oxidation of dihydroarnottin **5** with Osium tetroxide in a presence of *N*-methylmorpholine *N*-oxide (OsO<sub>4</sub>-NMO) as a sacrificial catalyst. Dihydroarnottin **5** was directly prepared by palladium-catalysed coupling of *o*-bromobenzoate (**4**) and 6,7-methylenedioxy-1-tetralone (**3**) using Buchwald protocol<sup>42</sup>. Dihydroarnottin **6** was subsequently hydroxylated with NBS and water to give **7**, then transformed into a methyl ether oxime **8** in the presence of methyl hydroxylamine-hydrochloric acid in pyridine. We found that, in some cases, bromination resulted in 3,4-dibromination (see experimental, **7**), in this case, we were able to selectively hydrolyse C-4 position to give a C-3-bromo-C4-hydrox-1- ketone, and the debromination was achieved by palladium catalysed reaction. Finally, 2-aryl-1,4-naphthoquinone-1-oxime methyl ethers **9** were obtained by IBX oxidation in DMSO at elevated temperatures. The 2-aryl-1,4-naphthoquinone-1-oxime were then treated with methyl iodide employing potassium carbonate as a base in DMF to achieve desired ester **10a**.



Scheme 2.1: Synthetic route of 2-aryl-1,4-naphthoquinone-1-oxime methyl ether.

The synthesis of the required ester **14** is depicted in Figure 2.1. It was envisaged that the commercially available phenol **11** would be the best starting point. The required ester **14** could be obtained from a suitably functionalised acid intermediate which can be obtained from ester **13**, via hydrolysis followed by esterification. The halogenated phenyl methyl ester **13** could be obtained from halogenation of the benzyl protected ether **12**, which in turn was obtainable from the commercially available phenol **11**.

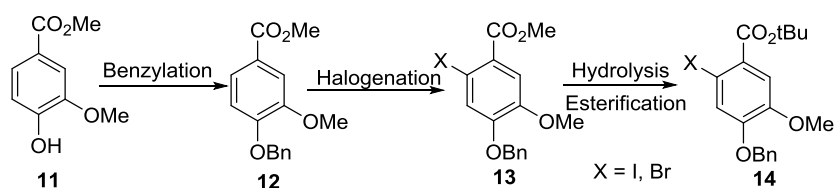


Figure 2.1: Synthetic procedure for ester **14**.

Thus the phenol **1** was subjected to etherification using the modified condition of Pouysegue et.al<sup>43</sup> employing benzyl bromide in DMF at elevated temperature of 100 °C, in the presence of potassium carbonate as an acid scavenger to give 100% the benzyl ether **2** after column chromatography (Scheme 2.2) which was confirmed by NMR 5.17 ppm, <sup>13</sup>C NMR at 71.04 ppm benzyl methylene peak. The Hathway et al<sup>44</sup> silver nitrate mediated halogenation conditions, failed to achieve neither iodate nor brominate the substrate, resulting in quantitative recovery of starting material and Further modifications (entry 2) also was inadequate to archive halogenated compound. Noteworthy, in the procedure by Carme Pampin et al<sup>45</sup>, when hypervalent iodide was employed (entry 3, and other case such as TMDACI<sup>46</sup>, not shown), resulted in the removal of the benzyl protecting group, resulting back to phenol **1**. Attempts to modify the procedure, by either varying the concentration of triflic acid or adjusting temperature proved inadequate.

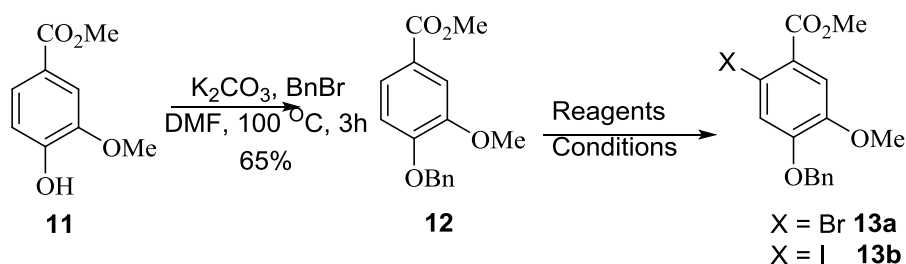
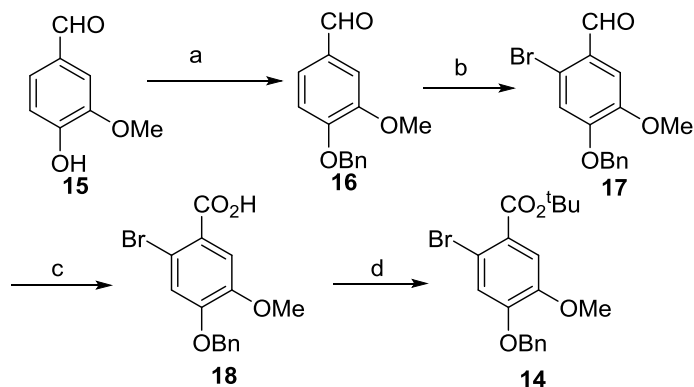


Table 2.1: Results from Halogenation of **12**

Entry	Reagents	Conditions	Results
1	AgNO <sub>3</sub> , I <sub>2</sub>	MeOH, 50°C, 12h	NR
2	AgNO <sub>3</sub> , I <sub>2</sub> , NaHCO <sub>3</sub>	MeOH, rt, 24h	NR
3	IPy <sub>2</sub> BF <sub>4</sub> , TfOH	DCM	<b>11</b>
4	AgNO <sub>3</sub> , Br <sub>2</sub>	MeOH, 50 °C, 24 h	NR

Scheme 2.2: Trials for the synthesis of ester **13a** or **14b**.

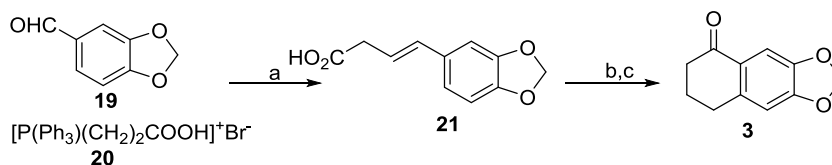
The above results prompted modification to the experimental procedure; it was assumed that the presence of electron withdrawing groups rendered the aryl group unreactive. Taking this to consideration, the commercially available aldehyde **15** (vanillin) was chosen as a starting point, opting to introduce the ester at later stage (Scheme 2.3).



Scheme 2.3: Reagents and Conditions. a)  $\text{K}_2\text{CO}_3$ , BnBr, DMF,  $100\text{ }^\circ\text{C}$ , 2h.; b)  $\text{AgNO}_3$ ,  $\text{Br}_2$ , MeOH, rt, 16h.; c)  $\text{NaH}_2\text{PO}_4$ ,  $\text{NaClO}_2$ ,  $\text{H}_2\text{O}_2$ ,  $\text{H}_2\text{O}$ , MeCN, rt, 2h.; d)  $\text{CCl}_3\text{C}(\text{NH})\text{O}^t\text{Bu}$ ,  $\text{BF}_3\cdot\text{Et}_2\text{O}$ , DCM-cyclohexane.

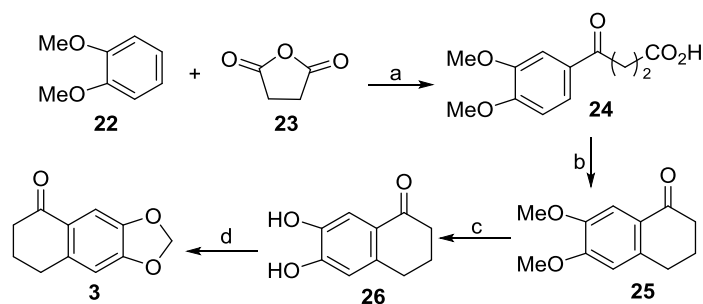
The revised approach, the synthesis of the benzyl ether **16** was performed similarly as above. Examining the halogenation of **16** employing the Hathway et. al procedure, were able to achieve the brominated compound **17** in good yield. Other general methods such as  $\text{AcOH}/\text{Br}_2$  were not successful, or giving low yield *ca.* 20% yield. Oxidation of the aldehyde **17** was achieved via Pinikin Oxidation procedure in excellent yield. In this procedure, upon disappearance of the starting aldehyde, the reaction was acidified with diluted (10%) HCl, then the crude acid obtained by extraction with EtOAc give crude acid **18** as a colorless solid, which was used in next step without further purification. Subjecting the crude acid to esterification conditions employing *t*-BuOH in the presence of catalytic amounts of  $\text{MgSO}_4$  resulted in recovery of the starting material without detection of the product. On the other hand, esterification using imidate in the presence of catalytic  $\text{BF}_3\cdot\text{Et}_2\text{O}$  gave the desired *t*-butyl ester **14b**, in satisfactory yield. We decided to optimize these conditions, and we found that increasing or decrease the lewis acid lowered the yield, but increasing the time length has a positive effect on the yield, 20 h being the optimum time.

We then turned our attention to the preparation of **3**. There are two procedures that were identified in literature. The first procedure is illustrated of scheme 2.4 below.



Scheme 2.4: Reagents and Conditions. a) NaH, DMSO-THF (1:1), rt, 24 h.; b)  $\text{H}_2$ , Pd/C, THF, rt, 3h.; c)  $\text{POCl}_3$ ,  $\text{K}_2\text{CO}_3$ , MeCN, 2h, rt

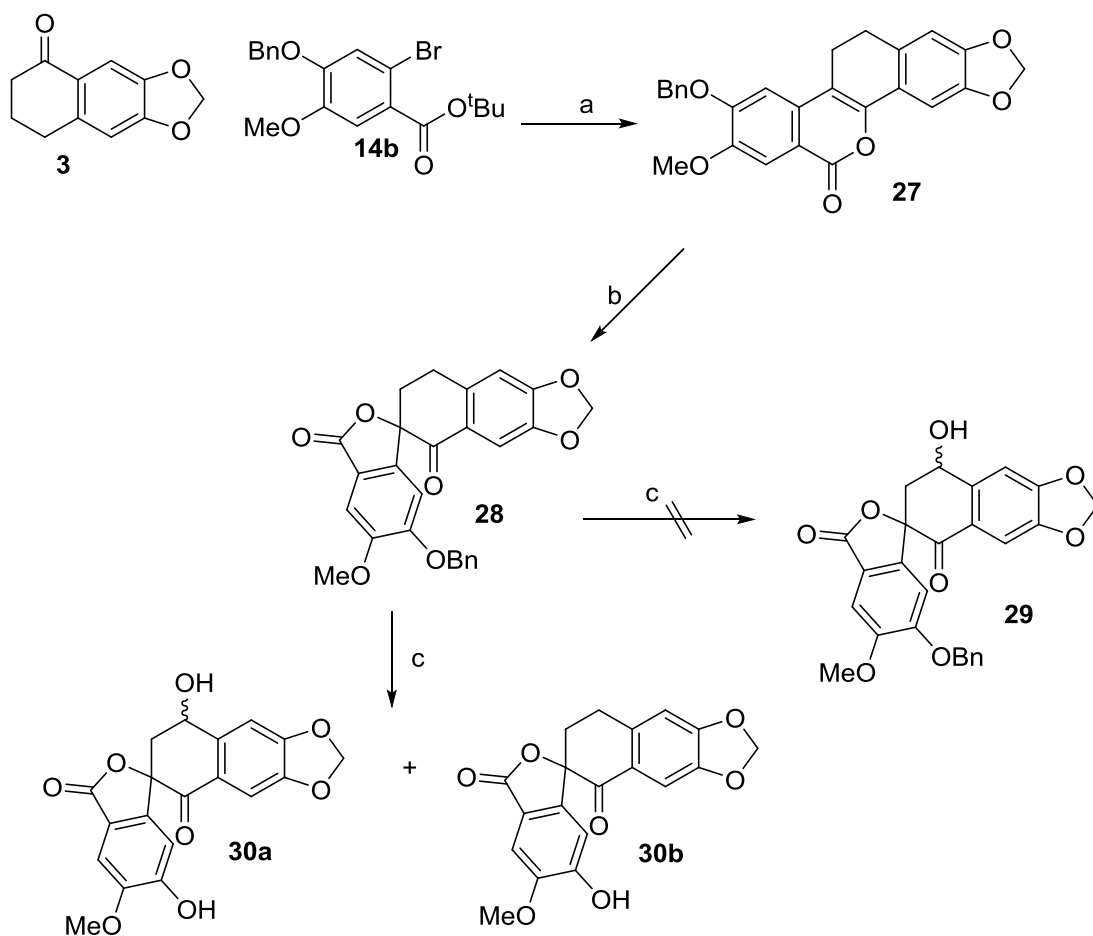
Compound **20**<sup>47</sup> was prepared by refluxing the commercially available propionic acid and triphenyl phosphine in CH<sub>3</sub>CN for 24 h in accordance with the published procedure, which was then subjected to the Wittig reaction of aldehyde **19** and the acid **20**, to give the desired enoic acid **21**. The enoic acid was reduced by palladium-mediated hydrogenation and upon filtration in Celite, without further purification the resulting crude product was subjected Friedel-Craft acylation with POCl<sub>3</sub><sup>48</sup>. All spectroscopic data were identical with reported. Unfortunately this procedure presented great difficulties in scaling up; hence we further examined an alternative method, as shown in Scheme 2.5.



Scheme 2.5: Reagents and Conditions. a) AlCl<sub>3</sub>, DCM, 40 °C, overnight.; b) 1) Pd/C (cat), H<sub>2</sub>, AcOH, rt, 24 h., 2) POCl<sub>3</sub>, K<sub>2</sub>CO<sub>3</sub>, MeCN, rt, 2h.; c) HBr, AcOH, 110 °C, 2h.; d) BrCH<sub>2</sub>Cl, Cs<sub>2</sub>CO<sub>3</sub>, 110 °C, 1.5 h.

The 1-tetralone **25** was synthesized employing the Haworth synthesis. Briefly, 1,2 methoxybenzene **22** was reacted with succinic anhydride **23** by a Friedel–Crafts acylation, the intermediate  $\gamma$ -keto acid **24** product was then reduced by palladium mediated hydrogenolysis, then a second Friedel–Crafts acylation mediated by POCl<sub>3</sub> gave product **25**, which was then subjected to de-methylation employing 30% HBr in Acetic acid at elevated temperatures to give the di-hydroxyl **26**. The product **26** was alkylated with bromochloromethane in DMF, to give the desired product **3**. We found this approach scalable to multi-gram scale and all spectroscopic data was compared to the published data.

We then synthesized dihydroarnottin I **27**, in a Palladium (Pd)-catalysed reaction in the presence of 2-bromobenzoate **14b** and 1-tetralone **3**. This was a key step to the reaction. Dihydroarnottin II **28** was achieved via OsO<sub>4</sub> oxidation in the presence of NMO as a cooxidant catalyst.

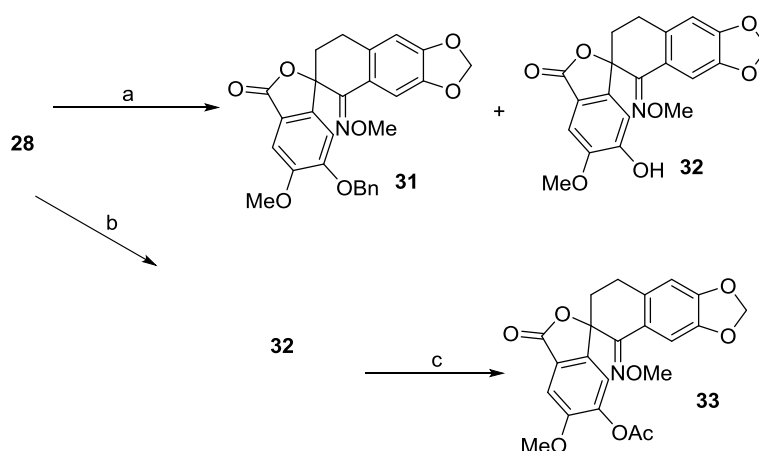


Scheme 2.6 : Reagents and Conditions. a) Pd(dba)<sub>3</sub>, Cs<sub>2</sub>CO<sub>3</sub>, Xantphos, Na<sub>2</sub>S<sub>2</sub>O<sub>5</sub>, toluene, 100 °C, 48 h, argon, 81%.; b) OsO<sub>4</sub>, NMO, CH<sub>2</sub>Cl<sub>2</sub>-acetone, r.t., 5 d, 86%.; c) (1) NBS, AIBN, benzene, 70 °C, 3 h; (2) acetone, H<sub>2</sub>O, 40 °C, 20 h, **30a**, 25%, **30b**, 40%.

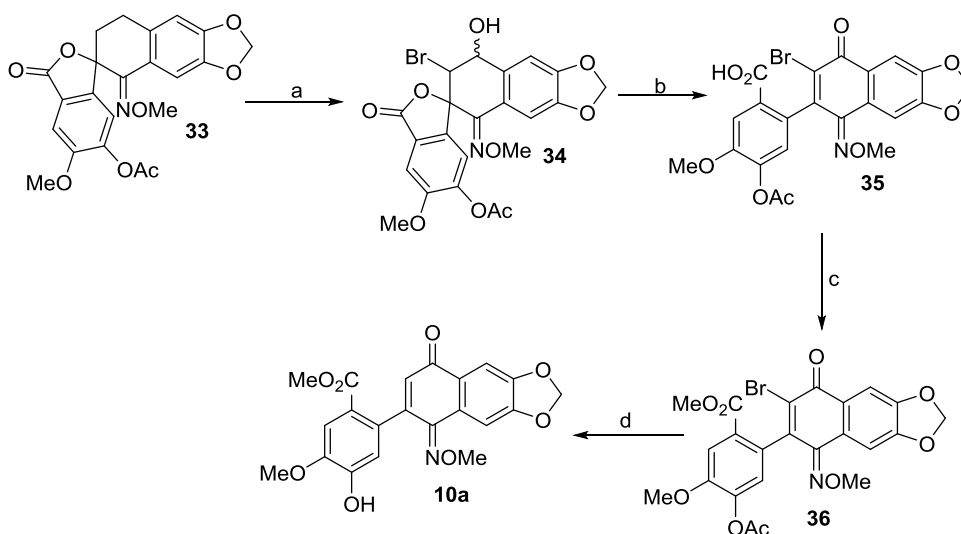
We encountered problems with hydroxylation of **28** as the desired product **29** was not observed rather other two products were observed, **30a** and **30b**. Detailed analyses showed that, de-benzylation occurred before hydroxylation. Selective protection studies indicated that, as expected, the secondary hydroxyl was more reactive than the phenol group. This implied that a laboratory intensive selective protecting and selective de-protection. While there was a possibility of changing the benzyl protecting group, we rather opted for oximation to be succeeded by hydroxylation.

Preliminary oximation (Figure 2.7) of the spiro tetralone **28** resulted in the benzylated **31** and non-benzylated **32** oximes, implying the instability of the benzyl ether both under radical and acidic conditions. We then decided to remove the benzyl ether under Palladium (Pd)-catalysed hydrolysis, resulting in many un-resolvable spots/poor yield. We found that, the same hypervalent iodide reagents (see Scheme 2.2), used earlier in attempting to iodinate **12**, works best. We then engaged

into optimizing this reaction exploring Aromatic benzyled-ethers (Ar-OBn) (results not shown). We found that the reactions satisfactory gave the end-product. During optimization, we found that the hypervalent iodide could be used catalytically in these conditions to give a pure product and furthermore, the reaction rate was directly proportion to amount of an acid used. Upon this discovery, we decided to perform a two-step reaction, de-benylation followed by oximation to achieve methyl oxime ether **32**. Upon acetylation of **32**, we then attempted hydroxyl group insertion, on the spiro oxime **33**, applying the aforementioned AIBN/NBS conditions. In an unexpected outcome, additional bromine-incorporated oxime **34** resulted (Scheme 2.8).



Scheme 2.7: Reagents and Conditions. a)  $\text{NH}_2\text{OME}\cdot\text{HCl}$ , pyridine,  $90^\circ\text{C}$ , 12 h, **31**, 20%, **33** 35%. b) (1)  $\text{TfOH}$ ,  $\text{IPy}_2\text{BF}_4$ ,  $\text{CH}_2\text{Cl}_2$ ,  $0^\circ\text{C}$ , 20 min; (2)  $\text{NH}_2\text{OME}\cdot\text{HCl}$ , pyridine,  $90^\circ\text{C}$ , 12 h 98%. c)  $\text{Ac}_2\text{O}$ ,  $\text{Et}_3\text{N}$ ,  $\text{I}_2$ ,  $\text{THF}$ ,  $40^\circ\text{C}$ , 7 h, 90%.



Scheme 2.8 : Reagents and Conditions. a) 1) NBS, AIBN, benzene, 70 °C, 3 h; 2) acetone, H<sub>2</sub>O, 40 °C, 20 h, 29%; b) 1) IBX, DMSO, 50 °C, 2 h; 2) Et<sub>3</sub>N, CH<sub>2</sub>Cl<sub>2</sub>, r.t., 2 h, 99%; c) MeI, K<sub>2</sub>CO<sub>3</sub>, DMF, r.t., 2 h, 65%; d) Pd(OAc)<sub>2</sub>, K<sub>2</sub>CO<sub>3</sub>, PPh<sub>3</sub>, BuOH, 100 °C, 2 h, 93%.

The 3-bromo-oxime **34** was then employed in the direct construction of the 1,4-naphthoquinone 1-oxime **35** by oxidation with hypervalent-iodine (IBX) in DMF at elevated temperatures. Conventional esterification of **35** with MeI and potassium carbonate in DMF gave ester **36**. Palladium mediated reductive debromination of **36** smoothly afforded the target 1,4-naphthoquinone 1-oxime **10a**.

#### Synthesis of conjugated-AK25

In the previous investigation for cytotoxicity of **10b**, it was determined that low solubility in DMSO resulted in limited potency. We then undertook to introduce an amino acid-based conjugated. We considered introducing glycine-; n = 2,  $\beta$ -alanine- and n = 3,  $\gamma$ -aminobutyric acid-based conjugated **10b**, as shown in Figure 2.2.

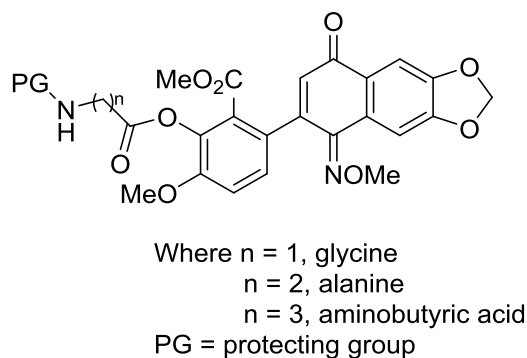


Figure 2.2: The synthetic conjugate.

Compound **10b** was synthesized as previously reported. We started by investigating the possibility of forming the conjugated salicylate **38** and employing N-protected glycine residue as show in Figure 2.3.

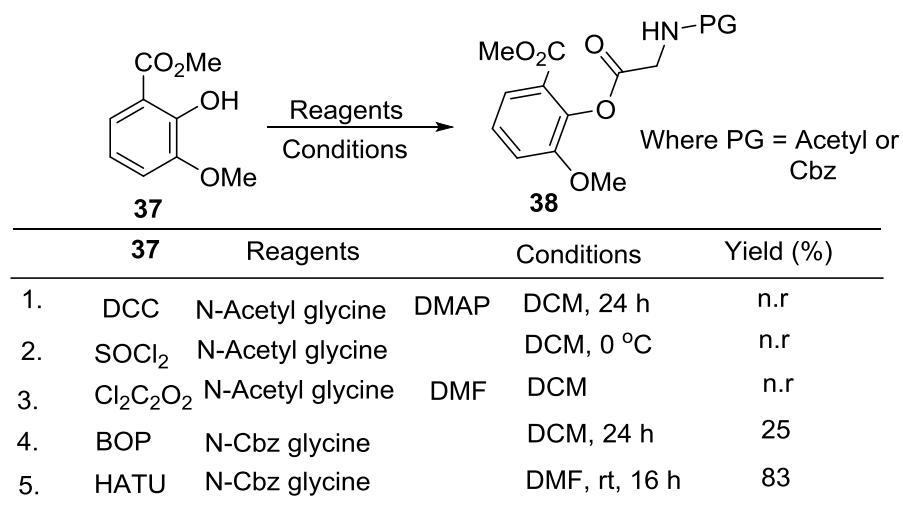
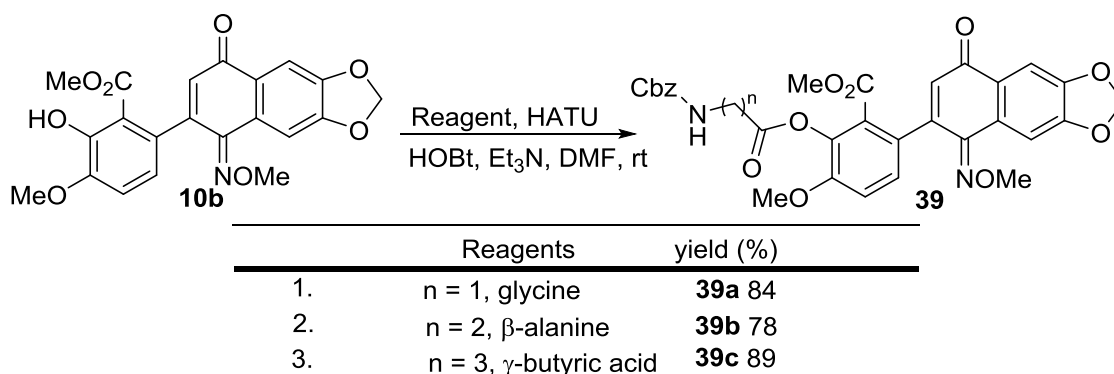


Figure 2.3: Model reaction for synthesis of conjugate **39** (below).

We found condensation with DCC in the presence of catalytic DMAP in-efficient, resulting in recovery of starting material. Similarly, acid chlorides from thionyl chloride and oxalyl chloride also resulted in no formation of the products after 24 h. BOP [(Benzotriazol-1-yloxy)tris(dimethylamino)phosphonium hexafluorophosphate] finally achieved the product but rather in unsatisfactory yield of 25%. To ease TLC analysis, we decided to employ the UV active N-Cbz-glycine. HATU further improved the yield, giving the product in 83% yield in 16 h at room temperature. We then decide to use these conditions for preparation of our conjugates.



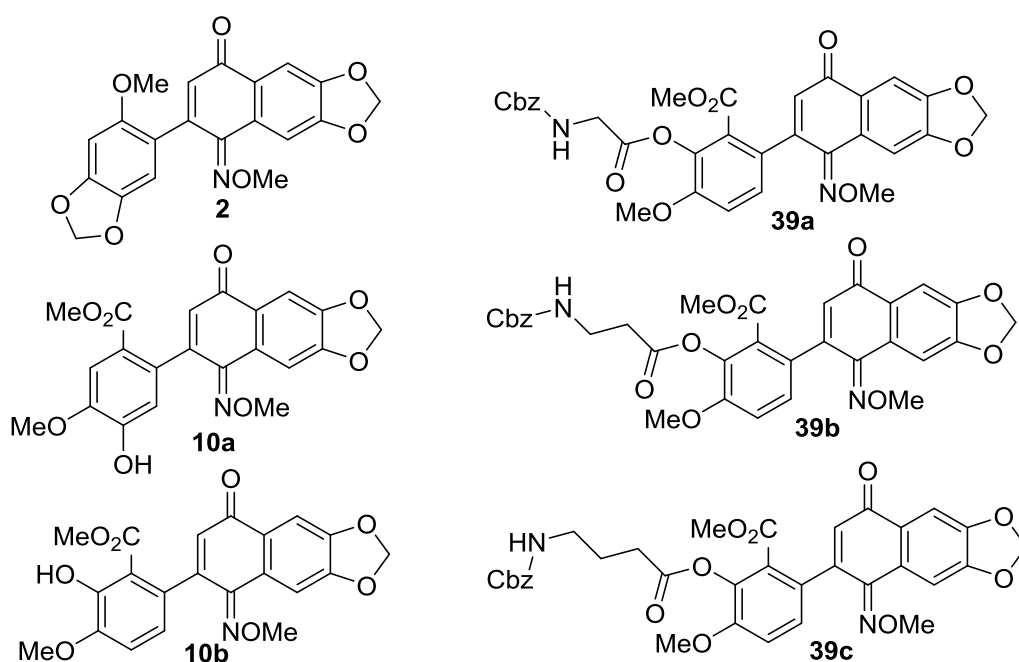
Scheme 2.9: Synthesis of conjugates **39 a-c** employing HATU.

Employing excess amount of the amino acid (2 eq), we were able to achieved satisfactory yields in all conjugates, glycine (84%), β-alanine (78%) and γ-butyric acid (89%). The conjugates showed an improved polarity, compared to it precursor **10b**. The conjugates could be de-protected but due to time constrains, we choose not to remove the Cbz-group. It would be worth to mention that we have hoped to form a water-soluble amine-hydrochloric acid (RNH<sub>2</sub>·HCl) type conjugate. The biological results would be discussed in the next section.

## Chapter 3

### Biologic Results

The synthesized compounds, **10a**, **39a**, **39b** and **39c** were evaluated *in vitro* as inhibitors of tubulin (de)-polymerization for Hela (cervix). The results are shown in table below.



Compound	IC <sub>50</sub> (μM)	Docking Score
<b>2</b>	0.104	56.04
<b>10a</b>	>10	60.69
<b>10b</b>	0.034	64.12
<b>39a</b>	5.32	N/A
<b>39b</b>	0.87	N/A
<b>39c</b>	3.58	N/A
Colchicine	0.024	57.59

Figure 3.1: Synthesized compounds and their biological activity.

The antiproliferative activities of the newly synthesized compounds were then tested against Hela cell lines. The *in vitro* activities, expressed as IC<sub>50</sub> values in micrograms per milliliter together with that of **31b**, the most active compound in previous *in vitro* tests and **2**, the lead compound. Compounds shown with IC<sub>50</sub> values greater than 10 (>10), showed low antiproliferative activities due to their poor solubility in aqueous solution which prevented a reliable evaluation of their *in vitro* activities. It is also worth mentioning that, in order to obtain comparable biological tests, experiments were performed and were all measured with same instruments. The percent of growth

and the inhibition exerted by different doses (0–10  $\mu$ M or LogM) are recorded.

Molecular modeling studies were performed with compounds **10a**, **10b** and **2** in order to investigate their possible interactions with the amino acid residues in the active site of colchicine binding site.

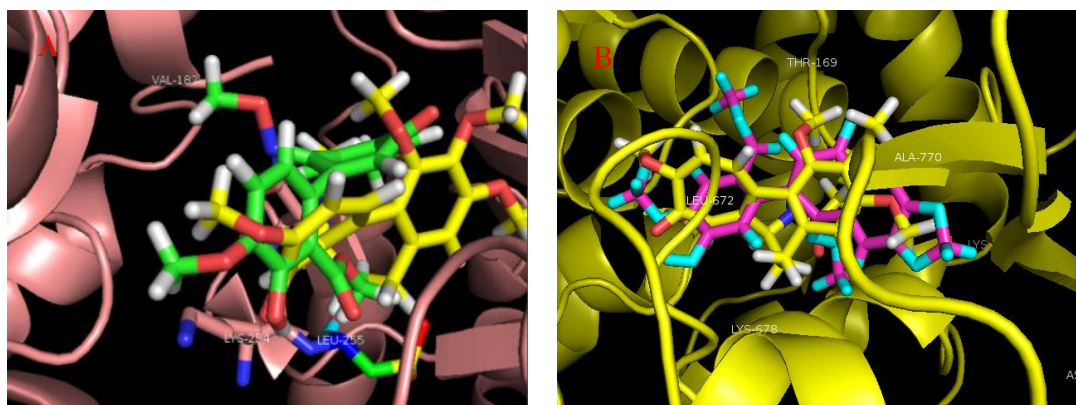


Figure 3.2: A) Binding of Colchicine (yellow) and **10a** (green), B) Binding of Colchicine (yellow) and **10b** (green).

Crystallographic structure of binding pocket residues of tubulin was obtained from protein database (pdb code: ISA0). The binding pocket of the colchicine has been very well described at the present. We then focused on the binding modes of the most active compound **31** to tubulin, compound **31** assumed a conformation in the same binding region of colchicine. The 2-aryl group of **31** was positioned in a similar orientation of the corresponding ring trimethoxy of the colchicine. The docking score of **31** (64.12) showed more potency than colchicine (57.59), hence we decided specific research on the binding of these aforementioned ligands (Figure 3B). Notably, both colchicine and **31** have hydrophobic interaction with leu255 and furthermore, both form a hydrogen interaction with lys254. The higher potency of **31** might be primarily due to differences in pKa of the phenol of **31** as oppose to the amide bond of the colchicine. The lower pKa of phenol increases the hydrogen bonding strength as it been observed in other cases<sup>49</sup>. Interestingly enough, **28** showed the highest affinity, with a mode almost similar to **31**, but the compound was biologically inactive.

## Chapter 4

### Experimental Section

#### Molecular Docking

X-ray crystal structure of  $\alpha/\beta$ tubulin (PDB code 1SA0) was retrieved for docking studies. The structure was used as obtained. In order to evaluate the interaction between the naphthoquinone derivatives and tubulin protein, we have executed the docking simulation using GOLD 3.2 (CCDC Software Ltd., Cambridge, UK). The three-dimensional structures of the naphthoquinone derivatives used in this study were optimized by semiempirical PM3 method. GoldScore was chosen as a fitness function and the standard default settings were used in all calculations. On the basis of score, top scored docking structures were visually inspected for each ligand. The molecular interactions were visualized by Pymol 1.3.

#### Cytotoxicity Assay

In vitro anticancer activity of compounds using MTT assay. Cytotoxicity testing in vitro was done by the method of Woerdenbag et al.<sup>1</sup>  $2 \times 10^3$  cells/well were incubated in the 5% CO<sub>2</sub> incubator for 24 h to enable them to adhere properly to the 96-well polystyrene microplate (Grenier, Japan). Test compound dissolved in 100% DMSO (Merck, Japan) in at least five doses was added and left for 6 h after which the compound plus media was replaced with fresh media and the cells were incubated for another 48 h in the CO<sub>2</sub> incubator at 37 °C. The concentration of DMSO used in our experiments never exceeded 0.1%, which was found to be non-toxic to cells. Then, 10  $\mu$ l MTT [3-(4,5-dimethylthiazol-2-yl)-2,5-diphenyltetrazolium bromide; Sigma] was added, and plates were incubated at 37 °C for 1 h. One hundred microlitres of dimethyl sulfoxide (DMSO, Merck, Japan) was added to all wells and mixed thoroughly. After a few minutes at room temperature to ensure that all crystals were dissolved, the plates were read on a SpectraMax 190 Microplate Elisa reader (Multiskan JX, labsystems) at 540 nm. Plates were normally read within 1 h of adding the DMSO. The experiment was done in triplicate and the inhibitory concentration (IC) values were calculated as follows:

$$\% \text{inhibition} = \frac{[1 - OD(540 \text{ nm}) \text{ of sample}]}{[OD(540 \text{ nm}) \text{ of control well}]} \times 100$$

IC<sub>50</sub> is the concentration  $\mu$ M required for 50% inhibition of cell growth as compared to that of untreated control

---

<sup>1</sup> Woerdenbag, H. J.; Moskal, T. A.; Pras, N.; Malingre, T. M.; el-Ferally, F. S.; Kampinga, H. H.; Konings, A. W. Cytotoxicity of artemisinin-related endoperoxides to Ehrlich ascites tumor cells. *J. Nat. Prod.* **1993**, *56*, 849-856.

## Chemistry

### General procedure

Unless noted otherwise, Reactions were carried out under argon atmosphere, all reagents and solvents we used as purchased without further purification. Analytical TLC was performed using silica gel 60 F<sub>254</sub> plates (Merck) or RP-18 F<sub>254s</sub> plates (Merck). Flash column chromatography was performed on silica gel 60 (70-230 mesh, Merck). <sup>1</sup>H-NMR (400 MHz) and <sup>13</sup>C-NMR (100 MHz) spectra were recorded on JEOL JNM ECP 400 in CDCl<sub>3</sub> unless otherwise stated. Coupling constants (*J*) are reported in hertz, and chemical shifts are reported in parts per million (δ) relative to CDCl<sub>3</sub> (7.26 ppm for <sup>1</sup>H and 77.00 ppm for <sup>13</sup>C). Melting points are uncorrected. IR spectra were recorded on a JASCO IR-300E spectrometer (ATR). High Resolution (HR)-FAB-MS and HR-electrospray ionization (ESI)-MS spectra were measured by JEOL JMS-HX 110A and JMS-T100LP and Thermo Scientific Exactive Bentitop Orbitrap spectrometers, respectively.

### **4-Benzyloxy-2-bromo-5-methoxybenzoic Acid (18)**

To a solution of 4-benzyloxy-2-bromo-5-methoxybenzaldehyde (1.18 g, 3.69 mmol) in MeCN (15 mL) was added a solution of NaH<sub>2</sub>PO<sub>4</sub> (0.133 g, 1.11 mmol) in H<sub>2</sub>O (3.7 mL) and H<sub>2</sub>O<sub>2</sub> (0.46 mL, 4.43 mmol), and then a solution of NaClO<sub>2</sub> (0.468 g, 5.17 mmol) in H<sub>2</sub>O (7.4 mL) was dropwise added under ice-cooling. After stirred at r.t. for 2h, the mixture was acidified with diluted HCl (pH *ca.* 3) and extracted with EtOAc (10 mL×2). The combined organic solutions were washed with H<sub>2</sub>O (10 mL×3) and brine (15 mL), dried (Na<sub>2</sub>SO<sub>4</sub>), and evaporated to give acid (1.17 g, 94%) as white solid. Mp: 182-183 °C (CH<sub>2</sub>Cl<sub>2</sub>); IR: 2923, 1683 cm<sup>-1</sup>; <sup>1</sup>H NMR: δ = 3.89 (s, 3H), 5.17 (s, 2H), 6.70 (br. s, 1H), 7.18 (s, 1H), 7.34-7.45 (m, 5H), 7.58 (s, 1H); <sup>13</sup>C NMR: δ = 56.2, 71.0, 115.0, 118.9, 121.7, 127.7, 128.5, 128.6, 135.5, 139.6, 148., 151.9, 169.5; HR(ESI)MS: *m/z* calcd for C<sub>15</sub>H<sub>14</sub>BrO<sub>4</sub>: 337.00755; found: 337.00909 .

### ***tert*-Butyl 4-Benzyloxy-2-bromo-5-methoxybenzoate (14b)**

To a stirred mixture of acid (0.300 g, 0.89 mmol) in CH<sub>2</sub>Cl<sub>2</sub> (1mL) was added a solution of *tert*-butyl 2,2,2-trichloroacetimidate (0.32 mL, 1.78 mmol) in cyclohexane (3 mL) at r.t. and a

small amount of  $\text{BF}_3 \cdot \text{OEt}_2$  (2 drops) after 5 min. The mixture was stirred at r.t. for 16 h, quenched with  $\text{H}_2\text{O}$  (10 mL), extracted with EtOAc (15 mL). The combined organic solutions were washed with brine (5 mL $\times$ 2), dried, and evaporated. Column chromatography of the residue (hexane : EtOAc = 5 : 1) afforded ester (0.437 g, 75%) as white powder, mp 115-116 °C. IR: 1702  $\text{cm}^{-1}$ ;  $^1\text{H}$  NMR:  $\delta$  = 1.61 (s, 9H), 3.89 (s, 3H), 5.14 (s, 2H), 7.10 (s, 1H), 7.31-7.43, (m, 6H);  $^{13}\text{C}$  NMR:  $\delta$  = 28.6, 56.2, 71.2, 82.4, 113.1, 114.5, 118.8, 125.8, 127.6, 128.4, 128.8, 135.9, 148.5, 150.8, 165.3; HR(ESI)MS: m/z calcd for  $\text{C}_{19}\text{H}_{22}\text{BrO}_4$ : 393.07015; found: 393.07015.

### **9-Benzyloxy-8-methoxy-2,3-methylenedioxy-6H-benzo[d]-3,4-dihydronaphtho[1,2-b]pyran-6-one (27)**

According to the reported procedure,<sup>6</sup> a mixture of bromobenzoate **14b** (65 mg, 0.166 mmol), tetralone **6** (38 mg, 0.200 mmol),  $\text{Pd}_2(\text{dba})_3$  (16 mg, 0.017 mmol), xantphos (19 mg, 0.033 mmol),  $\text{Cs}_2\text{CO}_3$  (163 mg, 0.500 mmol), and  $\text{Na}_2\text{S}_2\text{O}_5$  (3 mg, 0.017 mmol) in toluene (1 mL) was stirred at 100 °C for 36 h. Workup followed by washing the black-gray precipitate with  $\text{Et}_2\text{O}$  (5 mL  $\times$  4) afforded **27** as gray solid (69 mg, 81%). Mp 213-216 °C (EtOH); IR: 1748  $\text{cm}^{-1}$ ;  $^1\text{H}$  NMR:  $\delta$  = 2.75 (t,  $J$  = 8.4 Hz, 2H), 2.88 (t,  $J$  = 7.8 Hz, 2H), 5.29 (s, 2H), 5.96 (s, 2H), 6.68 (s, 1H), 6.94 (s, 1H), 7.32 (s, 1H), 7.33-7.50 (m, 5H), 7.69 (s, 1H);  $^{13}\text{C}$  NMR:  $\delta$  = 21.5, 27.6, 56.4, 71.2, 101.4, 103.5, 105.0, 107.8, 108.5, 110.6, 113.9, 122.9, 127.4, 128.5, 128.9, 130.9, 133.1, 136.0, 146.8, 147.5, 148.0, 149.5, 162.0; HR(ESI)MS: m/z calcd for  $\text{C}_{26}\text{H}_{20}\text{O}_6$ : 429.13381; found: 429.13476.

### **6,7-Methylenedioxy-1-tetralone-2-spiro-3'-(6-benzyloxy-7-methoxyphthalide) (28)**

According to the reported procedure,<sup>6</sup> a mixture composed of the lactone **27** (0.700 g, 1.63 mmol), a solution of  $\text{OsO}_4$  (0.041 g, 0.163 mmol), and NMO (0.951 g, 8.12 mmol) in acetone (7.5 mL) and  $\text{CH}_2\text{Cl}_2$  (7.5 mL) was stirred at r.t. for 5 days. After addition of  $\text{Na}_2\text{SO}_3$  (1.20 g, 8.12 mmol) workup

followed by column chromatography (hexane : EtOAc = 1 : 1) afforded spiro tetralone **28** as colorless solid (0.624 g, 86%). Mp 239-240 °C (EtOAc); IR: 1678 cm<sup>-1</sup>; <sup>1</sup>H NMR: δ = 2.35 (ddd, *J* = 13.7, 5.8, 5.8 Hz, 1H), 2.60 (ddd, *J* = 13.7, 8.6, 5.2 Hz, 1H), 2.99 (ddd, *J* = 17.8, 8.6, 5.2 Hz, 1H), 3.21 (ddd, *J* = 17.6, 5.8, 5.8 Hz, 1H), 3.94 (s, 3H), 5.08 (d, *J* = 10 Hz, 1H), 5.16 (d, *J* = 11 Hz, 1H), 6.08 (s, 1H), 5.16 (s, 1H), 6.63 (s, 1H), 6.72 (s, 1H), 7.27-7.34 (m, 6H), 7.41 (s, 1H); <sup>13</sup>C NMR: δ = 26.2, 33.9, 56.5, 71.4, 85.8, 102.4, 106.3, 107.2, 107.6, 108.2, 118.6, 125.9, 127.3, 128.4, 128.8, 135.8, 140.3, 142.4, 147.8, 151.7, 153.3, 153.7, 169.9, 188.7; HR(ESI)MS: *m/z* calcd for C<sub>26</sub>H<sub>20</sub>NaO<sub>7</sub>: 467.11067; found: 467.10307.

**1-Methoxyimino-6,7-methylenedioxy-1,2,3,4-tetrahydronaphthalene-2-spiro-3-(6-hydroxyl-7-methoxyphthalide) (32)**

A mixture of triflic acid (0.21 mL, 2.37 mmol) in DCM (1 mL), was dropwise added to an ice-cooled solution of **28** (0.351 g, 0.790 mmol) and IPy<sub>4</sub>BF<sub>4</sub> (0.059 g, 0.158 mmol) in CH<sub>2</sub>Cl<sub>2</sub> (30 mL). The mixture was stirred at 0 °C for 20 min, quenched with ice-H<sub>2</sub>O (20 mL), and extracted with CH<sub>2</sub>Cl<sub>2</sub> (15 mL). The combined organic solutions were washed with brine (20 mL×2), dried, and evaporated. The brownish oily residue was dissolved in pyridine (30 mL) and NH<sub>2</sub>OMe.HCl (0.659 g, 7.896 mmol) was added. The mixture was stirred at 90 °C for overnight, quenched with saturated solution of CuSO<sub>4</sub> in H<sub>2</sub>O (50 mL), and extracted with EtOAc (20 mL×3). The combined organic solutions were washed with H<sub>2</sub>O (20 mL) and brine (20 mL), dried, and evaporated. Column chromatography of the residue (hexane : EtOAc = 5 : 2) afforded **32** (0.298 g, 98%) as gum. IR: 3420, 1747 cm<sup>-1</sup>; <sup>1</sup>H NMR: δ = 2.09 (m, 2H), 2.80 (ddd, *J* = 16.0, 5.8, 3.8 Hz, 1H), 3.03 (ddd, *J* = 15.2, 10.4, 4.2 Hz, 1H), 3.61 (s, 3H), 3.99 (s, 3H), 5.96 (s, 1H), 5.98 (s, 1H), 6.66 (s, 1H), 6.80 (s, 1H), 7.31 (s, 1H), 7.40 (s, 1H), 8.60 (br. s, 1H); <sup>13</sup>C NMR: δ = 26.2, 37.9, 56.3, 62.7, 82.5, 101.1, 105.2, 106.3, 107.6, 117.8, 124.0, 133.5, 145.3, 147.1, 147.6, 147.9, 149.1, 151.8, 170.6, 171.1; HR(ESI)MS: *m/z* calcd for

C<sub>20</sub>H<sub>18</sub>NO<sub>7</sub>: 384.10833; found: 384.10868 .

**1-Methoxyimino-6,7-methylenedioxy-1,2,3,4-tetrahydronaphthalene-2-spiro-3-(6-acetyloxy-7-methoxyphthalide) (33)**

A solution of **32** (0.142 g, 0.367 mmol), Et<sub>3</sub>N (0.51 mL, 3.67 mmol), Ac<sub>2</sub>O (0.35 mL, 3.67 mmol), and catalytic amount of iodine (~5mg) in THF (3 mL) was stirred at 40 °C for 7 h, diluted with saturated solution of Na<sub>2</sub>S<sub>2</sub>O<sub>3</sub> in H<sub>2</sub>O (10 mL), and extracted with EtOAc (5 mL×3). The combined organic solutions were washed with brine (10 mL), dried, and evaporated. Column chromatography of the residue (EtOAc : hexane = 2 : 3) afforded **33** (0.141g, 90%) as a light-brown oil. IR: 1764 cm<sup>-1</sup>; <sup>1</sup>H NMR: δ = 2.30 (s, 3H), 3.60 (s, 3H), 3.91 (s, 3H), 5.95 (s, 1H), 5.97 (s, 1H), 6.65 (s, 1H), 6.99 (s, 1H), 7.39 (s, 1H), 7.43 (s, 1H); <sup>13</sup>C NMR: δ = 20.4, 26.3, 37.9, 56.4, 62.9, 82.7, 101.4, 105.0, 107.8, 108.0, 115.6, 123.8, 124.8, 133.4, 144.8, 145.4, 147.2, 149.2, 152.4, 168.3, 169.9, 171.1; HR(ESD)MS m/z: Calcd for C<sub>22</sub>H<sub>20</sub>NO<sub>8</sub>: 426.11889; found: 426.11978

**1-Methoxyimino-3-bromo-4-hydroxy-6,7-methylenedioxy-1,2,3,4-tetrahydronaphthalene-2-spiro-3-(6-acetyloxy-7-methoxyphthalide) (34)**

A mixture of **33** (222 mg, 0.521mmol), NBS (185. mg, 1.042 mmol), AIBN (9 mg, 0.052 mmol) in benzene (10 mL) was stirred at 70 °C for 3h and diluted with EtOAc (15mL). The mixture was washed with H<sub>2</sub>O (10 ml x 2) and brine (10 mL), dried, and evaporated. The reddish yellow residue was dissolved in acetone-H<sub>2</sub>O (3 : 1, 10 mL). After stirred at 40 °C for 20 h the mixture was diluted with EtOAc (15 mL), washed with H<sub>2</sub>O (10 mL×3) and brine (10 mL), dried, and evaporated. Column chromatography of the residue (EtOAc : hexane = 1 : 1) afforded **34** (77 mg, 29 %) as a yellow oil. IR: 3438, 1771cm<sup>-1</sup>; <sup>1</sup>H NMR: δ = 2.37 (s, 3H), 3.35 (br. s, 1H), 3.91 (s, 3H), 3.93 (s, 3H), 4.43 (d, *J* = 2.8 Hz, 1H), 4.99 (br. s, 1H), 6.07 (s, 2H), 7.10 (s, 1H), 7.41 (s, 1H), 7.48 (s, 1H), 7.98 (s,

1H);  $^{13}\text{C}$  NMR:  $\delta = 20.9, 55.3, 56.6, 63.6, 73.7, 86.7, 102.1, 107.5, 110.2, 110.4, 119.3, 121.8, 124.2, 131.6, 140.3, 144.5, 147.9, 150.0, 153.5, 167.3, 168.3, 171.5$ ; HR(ESI)MS  $m/z$ : Calcd for  $\text{C}_{22}\text{H}_{19}^{81}\text{BrNO}_9$ : 522.02227; found: 522.02488

**6-[2-(3-Bromo-1-methoxyimino-6,7-methylenedioxy-4-oxo-1,4-dihydronaphthyl)]-4-hydroxy-3-methoxybenzoic Acid (35)**

A solution of **34** (46 mg,  $6.9 \times 10^{-2}$  mmol) and IBX (39 mg,  $1.38 \times 10^{-1}$  mmol) in DMSO (1 mL) was stirred at 50 °C for 2h, quenched with  $\text{H}_2\text{O}$  (5 mL), and extracted with EtOAc (5 mL $\times$ 3). The combined organic solutions were washed with  $\text{H}_2\text{O}$  (10 mL) and brine (10 mL), dried, and evaporated. The residue was dissolved in  $\text{CH}_2\text{Cl}_2$  (5 mL), stirred at r.t. for 2 h after addition of  $\text{Et}_3\text{N}$  (19  $\mu\text{L}$ ,  $1.38 \times 10^{-1}$  mmol) under ice-cooling, and extracted with solution of 30% aq.  $\text{Na}_2\text{CO}_3$  (5 mL $\times$ 3). The combined aqueous solutions were acidified with 10% HCl (pH ca 3) and extracted with EtOAc (5 mL $\times$ 3). The combined organic solutions were dried and evaporated. Column chromatography of the residue (EtOAc:*n*-hex = 2:3 ) afforded **35** (36 mg, 99%) as yellow oil of 1:10 of (1'Z,3'E)- and (1'E,3'E). IR: 1768, 1647, 1609  $\text{cm}^{-1}$ ;  $^1\text{H}$  NMR for major isomer:  $\delta = 2.34$  (s, 3H), 3.94 (s, 3H), 3.95 (s, 3H), 6.13 (s, 1H), 6.16 (s, 1H), 6.94 (s, 1H), 7.70 (s, 1H), 7.76 (s, 1H), 8.32 (s, 1H);  $^{13}\text{C}$  NMR for major isomer:  $\delta = 21.0, 56.3, 65.1, 102.8, 107.6, 110.1, 114.6, 124.2, 125.2, 126.3, 127.4, 133.4, 143.3, 146.6, 149.7, 151.2, 151.3, 152.0, 168.4, 177.3$ ; HR(ESI)MS:  $m/z$  calcd for  $\text{C}_{22}\text{H}_{17}^{81}\text{BrNO}_9$ : 520.00662; found: 520.00472

**Methyl**

**6-[2-(3-Bromo-1-methoxyimino-6,7-methylenedioxy-4-oxo-1,4-dihydronaphthyl)]-4-hydroxy-3-methoxybenzoate (36)**

A mixture of **35** (19 mg,  $3.67 \times 10^{-2}$  mmol), MeI (5  $\mu\text{L}$ ,  $7.27 \times 10^{-2}$  mmol), and  $\text{K}_2\text{CO}_3$  (10 mg,

7.27×10<sup>-2</sup> mmol) in DMF (1 mL) was stirred at r.t. for 2 h, quenched with H<sub>2</sub>O (5 mL), and extracted with EtOAc (3 mL×3). The combined organic solutions were washed with saturated solution of NaHCO<sub>3</sub> in H<sub>2</sub>O (5 mL) and brine (5 mL), dried, and evaporated. Column chromatography of the yellow residue (hexane : EtOAc = 2 : 3) afforded **36** (13 mg, 65%) as yellow oil of 1:10 of (1'Z,3'E)- and (1'E,3'E). IR: 1721, 1648 cm<sup>-1</sup>; <sup>1</sup>H NMR for major isomer: δ = 2.33 (s, 3H), 3.70 (s, 3H), 3.95 (s, 3H), 3.96 (s, 3H), 6.12 (s, 2H), 6.95 (s, 1H), 7.66 (s, 1H), 7.77 (s, 1H), 8.34 (s, 1H); <sup>13</sup>C NMR for major isomer: δ = 20.7, 52.5, 56.1, 64.9, 102.4, 107.2, 110.0, 113.7, 124.5, 124.8, 125.8, 127.3, 132.5, 142.5, 146.4, 149.7, 150.6, 151.2, 151.9, 165.7, 168.3, 177.0; HR(ESI)MS m/z: calcd. for C<sub>23</sub>H<sub>19</sub><sup>81</sup>BrNO<sub>9</sub>: 534.02227; found: 534.01988.

## Methyl

### 4-Hydroxy-3-methoxy-6-[2-(1-methoxyimino-6,7-methylenedioxy-4-oxo-1,4-dihydronaphthyl)]benzoate (**10a**)

A mixture of **36** (7 mg, 1.3×10<sup>-3</sup> mmol), Pd(OAc)<sub>2</sub> (0.15 mg, 7×10<sup>-5</sup> mmol), and Ph<sub>3</sub>P (0.7 mg, 2.6×10<sup>-4</sup> mmol) in *n*-BuOH (3 mL) was stirred at 100 °C for 2 h under nitrogen atmosphere, diluted with EtOAc (6 mL), and filtered through Celite pad. The filtrate was washed with H<sub>2</sub>O (3 mL×2) and brine (3 mL), dried, and evaporated. Column chromatography of the residue (SiO<sub>2</sub>, EtOAc : hexane = 1 : 1) afforded **10a** (5.1 mg, 93%) as light-yellow solid, mp 89-91 °C. IR (ATR): 3437, 1771 cm<sup>-1</sup>; <sup>1</sup>H NMR (400 MHz, CDCl<sub>3</sub>) for (Z)-isomer: δ = 3.64 (s, 3H), 3.97 (s, 3H), 4.00 (s, 3H), 6.12 (s, 2H), 6.49 (s, 1H), 6.91 (s, 1H), 7.49 (s, 1H), 7.70 (s, 1H), 8.35 (s, 1H); <sup>13</sup>C NMR (100 MHz, CDCl<sub>3</sub>) for (Z)-isomer: δ = 52.2, 56.4, 64.5, 102.3, 106.4, 110.2, 112.4, 116.6, 123.1, 124.6, 127.3, 129.0, 133.2, 146.1, 146.5, 148.7, 149.5, 151.5, 153.4, 167.1, 183.6; HRMS(ESI): m/z calcd for C<sub>21</sub>H<sub>17</sub>NNaO<sub>8</sub>: 434.08519; found: 434.08329.

General procedure for preparation of compounds **39a-c**.

A mixture of NCbz-protected amino acid (3 eq), Et<sub>3</sub>N (2 eq), and HATU (3 eq) in DMF (3 mL) was stirred at r.t. for 1 h, followed by **10b** and HOBt (1 eq) and further stirred for 18 h at rt. The reaction was quenched with H<sub>2</sub>O (5 mL), and extracted with EtOAc (3 mLx3). The combined organic solutions were washed with saturated solution of NaHCO<sub>3</sub> in H<sub>2</sub>O (3 mLx 2) and brine (3 mL), dried over MgSO<sub>4</sub>, and evaporated. Column chromatography of the resulted residue (hexane : EtOAc = 3 : 2) afforded **39a-c**.

**39a Methyl 6-[2-(1-methoxyimino-6,7-methylenedioxy-4-oxo-1,4-dihydronaphthyl)]-2-(N-Cbz-gly-O)-3-methoxybenzoate**

84 % Yield. IR (ATR): 3437, 1771, 1760 cm<sup>-1</sup>; <sup>1</sup>H NMR (400 MHz, CDCl<sub>3</sub>) : δ = 3.61 (s, 3H), 3.89 (s, 3H), 4.01 (s, 3H), 4.32 (s, 2H), 5.16 (s, 2H), 5.32 (s, 1H), 6.12 (s, 2H), 6.59 (s, 1H), 7.01 (s, 1H), 7.25 (s, 3H), 7.38 (s, 2H), 7.70 (s, 1H), 8.35 (s, 1H); <sup>13</sup>C NMR (100 MHz, CDCl<sub>3</sub>) δ 56.3, 64.7, 102.2, 106.2, 109.8, 113.8, 128.0, 128.1, 128.2, 128.6, 130.0, 136.3, 137.8, 145.1, 149.5, 151.4, 152.0, 163.6, 165.3, 167.8, 183.4; HRMS(ESI): m/z calcd for C<sub>31</sub>H<sub>26</sub>N<sub>2</sub>NaO<sub>11</sub>: 625.144404; found: 625.14343.

**39b Methyl 6-[2-(1-methoxyimino-6,7-methylenedioxy-4-oxo-1,4-dihydronaphthyl)]-2-(N-Cbz-β-ala-O)-3-methoxybenzoate**

Prepared similarly to compound **39a**

78 % Yield, IR (ATR): 3437, 1771, 1760 cm<sup>-1</sup>; <sup>1</sup>H NMR (400 MHz, CDCl<sub>3</sub>) : δ = 2.89 (s, 2H), 3.50 (s, 3H), 3.66 (s, 2H), 3.89 (s, 3H), 4.01 (s, 3H), 5.12 (s, 2H), 5.72 (s, 1H), 6.12 (s, 2H), 6.60 (s, 1H), 7.01 (s, 1H), 7.35 (s, 6H), 7.70 (s, 1H), 8.33 (s, 1H); <sup>13</sup>C NMR (100 MHz, CDCl<sub>3</sub>) δ 33.7, 36.8, 52.2, 56.2, 64.7, 66.7, 102.2, 106.2, 109.8, 113.8, 124.0, 127.6, 128.0, 128.1, 128.4, 128.5, 128.6, 130.0, 132.1, 136.5, 137.9, 144.9, 149.4, 151.5, 151.8, 156.3, 156.4, 165.5, 169.6, 183.4; HRMS(ESI): m/z calcd for C<sub>32</sub>H<sub>28</sub>N<sub>2</sub>NaO<sub>11</sub>: 639.15758; found: 639.15908.

**39c**

**Methyl**

**6-[2-(1-methoxyimino-6,7-methylenedioxy-4-oxo-1,4-dihydronaphthyl)]-2-(N-Cbz- $\gamma$ -butyric acid-*O*-)3-methoxybenzoate**

Prepared similarly to compound **39a**

89 % Yield, IR (ATR): 3437, 1771, 1760  $\text{cm}^{-1}$ ;  $^1\text{H}$  NMR (400 MHz,  $\text{CDCl}_3$ ):  $\delta$  = 2.00 (s, 2H), 2.67 (m, 2H), 3.36 (s, 2H) 3.50 (s, 3H), 3.88 (s, 3H), 4.01 (s, 3H), 5.10 (s, 2H), 5.18 (s, 1H), 6.12 (s, 2H), 6.60 (s, 1H), 7.01 (s, 1H), 7.35 (s, 6H), 7.70 (s, 1H), 8.33 (s, 1H);  $^{13}\text{C}$  NMR (100 MHz,  $\text{CDCl}_3$ )  $\delta$  17.5, 24.7, 30.9, 32.8, 40.0, 46.4, 52.2, 56.2, 64.7, 66.7, 68.0, 102.2, 106.2, 109.7, 113.5, 124.0, 127.7, 127.9, 128.1, 128.2, 128.4, 128.5, 128.6, 130.0, 136.5, 138.4, 144.9, 149.5, 151.4, 151.5, 152.0, 156.5, 165.5, 170.6, 183.4; HRMS(ESI):  $m/z$  calcd for  $\text{C}_{33}\text{H}_{30}\text{N}_2\text{KO}_{11}$ : 669.15103; found: 669.14867.

## Chapter 5

### Conclusion

Four 2-aryl-1,4-naphthoquinone synthesized were biologically active in vitro antitumor studies. Compounds (**39a-c**)-type may be potent drug candidates and their potency may be increased with relatively simple structural changes in the 2-aryl group, hence aiding to the insight to future optimization of the series.

S Mkhize, N Suzuki, A Kurosawa, M Fujinami, C Chaicharoenpong, T Ishikawa; New Synthestic Procedure for 2-Aryl-1,4-naphthoquinone-1-oxime Methyl Ethers with Potent Antitumor Activity, *Synlett*, **2014**, *25*, 2059-2063

Evaluation Committee Members

Chairman: Professor Masami Ishibashi

Member : Professor Atsushi Nishida

Professor Yasushi Arano

## References.

- (1) IARC. *World Cancer Report*; 2012.
- (2) Jordan, M. A.; Wilson, L. *Nat. Rev. Cancer* **2004**, *4*, 253.
- (3) Jordan, M. A.; Wendell, K.; Gardiner, S.; Derry, W. B.; Copp, H.; Wilson, L. *Cancer Res.* **1996**, *56*, 816.
- (4) Jordon Mary Ann; Wilson Leslie. *Taxane Anticancer Agents*; Georg, G. I.; Chen, T. T.; Ojima, I.; Vyas, D. M., Eds.; ACS Symposium Series; American Chemical Society: Washington, DC, 1994; Vol. 583, pp. 138–153.
- (5) Nogales, E. *Annu. Rev. Biochem.* **2000**, *69*, 277.
- (6) Siegrist, S. E.; Doe, C. Q. *Genes Dev.* **2007**, *21*, 483.
- (7) Wilson, L.; Jordan, M. A. *Chem. Biol.* **1995**, *2*, 569.
- (8) Kirschner, M.; Mitchison, T. *Cell* **1986**, *45*, 329.
- (9) Panda, D.; Miller, H. P.; Wilson, L. *Biochemistry* **2002**, *41*, 1609.
- (10) Howard, J.; Hyman, A. A. *Nature* **2003**, *422*, 753.
- (11) Chen, W.; Zhang, D. *Nat. Cell Biol.* **2004**, *6*, 227.
- (12) Wilson, L.; Panda, D.; Jordan, M. A. *Cell Struct. Funct.* **1999**, *24*, 329.
- (13) Honore, S.; Pasquier, E.; Braguer, D. *Cell. Mol. Life Sci.* **2005**, *62*, 3039.
- (14) Lu, Q.; Luduena, R. F. *J. Biol. Chem.* **1994**, *269*, 2041.
- (15) Verdier-Pinard, P.; Wang, F.; Burd, B.; Angeletti, R. H.; Horwitz, S. B.; Orr, G. A. *Biochemistry* **2003**, *42*, 12019.
- (16) Pasquier, E.; Kavallaris, M. *IUBMB Life* **2008**, *60*, 165.

- (17) Chang, W.; Gruber, D.; Chari, S.; Kitazawa, H.; Hamazumi, Y.; Hisanaga, S.; Bulinski, J. C. *J. Cell Sci.* **2001**, *114*, 2879.
- (18) Carazo-Salas, R. E.; Gruss, O. J.; Mattaj, I. W.; Karsenti, E. *Nat. Cell Biol.* **2001**, *3*, 228.
- (19) Rusan, N. M.; Fagerstrom, C. J.; Yvon, A. M.; Wadsworth, P. *Mol. Biol. Cell* **2001**, *12*, 971.
- (20) Maddox, P.; Desai, A.; Oegema, K.; Mitchison, T. J.; Salmon, E. D. *Curr. Biol.* **2002**, *12*, 1670.
- (21) Nicklas, R. B.; Ward, S. C.; Gorbisky, G. J. *J. Cell Biol.* **1995**, *130*, 929.
- (22) Weaver, B. A. A.; Cleveland, D. W. *Cancer Cell* **2005**, *8*, 7.
- (23) Conde, C.; Cáceres, A. *Nat. Rev. Neurosci.* **2009**, *10*, 319.
- (24) Jordan, M. A. *Curr. Med. Chem. Anticancer. Agents* **2002**, *2*, 1.
- (25) Jiménez-Barbero, J.; Amat-Guerri, F.; Snyder, J. P. *Curr. Med. Chem. Anticancer. Agents* **2002**, *2*, 91.
- (26) Ngan, V. K.; Bellman, K.; Panda, D.; Hill, B. T.; Jordan, M. A.; Wilson, L. *Cancer Res.* **2000**, *60*, 5045.
- (27) Jordan, M. A.; Toso, R. J.; Thrower, D.; Wilson, L. *Proc. Natl. Acad. Sci. U. S. A.* **1993**, *90*, 9552.
- (28) Noble, R. L.; Beer, C. T.; Cutts, J. H. *Biochem. Pharmacol.* **1959**, *1*, 347.
- (29) Bai, R. L.; Pettit, G. R.; Hamel, E. *J. Biol. Chem.* **1990**, *265*, 17141.
- (30) Derry, W. B.; Wilson, L.; Jordan, M. A. *Biochemistry* **1995**, *34*, 2203.
- (31) Hastie, S. B. *Pharmacol. Ther.* **1991**, *51*, 377.
- (32) Slaninová, I.; Slunská, Z.; Šinkora, J.; Vlková, M.; Táborská, E. **2007**, *45*, 131.
- (33) D Walterová I Válka, J Vicar, C Vavrecková, E Táborská, R J Harjrader, D L Meyer, H Cerná, V Simánek, J. U. *Acta Univ. Palacki. Olomuc. Fac. Med.* **1995**, *139*, 7.

- (34) Ishikawa, T.; Saito, T.; Kurosawa, A.; Watanabe, T.; Maruyama, S.; Ichikawa, Y.; Yamada, R.; Okuzawa, H.; Sato, H.; Ueno, K. *Chem. Pharm. Bull. (Tokyo)*. **2011**, *59*, 472.
- (35) Ishikawa, T.; Ishii, H. *Heterocycles* **1999**, *50*, 627.
- (36) Tillequin, F. *Phytochem. Rev.* **2007**, *6*, 65.
- (37) Choi, W. Y.; Jin, C. Y.; Han, M. H.; Kim, G. Y.; Kim, N. D.; Lee, W. H.; Kim, S. K.; Choi, Y. H. *Anticancer Res.* **2009**, *29*, 4457.
- (38) Slavík, J.; Slavíková, L. *Collect. Czechoslov. Chem. Commun.* **1955**, *20*, 356.
- (39) Ishikawa, T.; Saito, T.; Ishii, H. *Tetrahedron* **1995**, *51*, 8447.
- (40) Sato, H.; Yamada, R.; Yanagihara, M.; Okuzawa, H.; Iwata, H.; Kurosawa, A.; Ichinomiya, S.; Suzuki, R.; Okabe, H.; Yano, T.; Kumamoto, T.; Suzuki, N.; Ishikawa, T.; Ueno, K. *J. Pharmacol. Sci.* **2012**, *118*, 467.
- (41) Konno, F.; Ishikawa, T.; Kawahata, M.; Yamaguchi, K. *J. Org. Chem.* **2006**, *71*, 9818.
- (42) Fox, J. M.; Huang, X.; Chieffi, A.; Buchwald, S. L. *J. Am. Chem. Soc.* **2000**, *122*, 1360 .
- (43) Pouységou, L.; Avellan, A.-V.; Quideau, S. *J. Org. Chem.* **2002**, *67*, 3425.
- (44) Hathaway, B. A.; White, K. L.; McGill, M. E. *Synth. Commun.* **2007**, *37*, 3855.
- (45) Carme Pampín, M.; Estévez, J. C.; Estévez, R. J.; Maestro, M.; Castedo, L. *Tetrahedron* **2003**, *59*, 7231.
- (46) Hajipour, A. R.; Arbabian, M.; Ruoho, A. E. *J. Org. Chem.* **2002**, *67*, 8622.
- (47) Ahmed, R.; Altieri, A.; D'Souza, D. M.; Leigh, D. A.; Mullen, K. M.; Pappmeyer, M.; Slawin, A. M. Z.; Wong, J. K. Y.; Woollins, J. D. *J. Am. Chem. Soc.* **2011**, *133*, 12304.
- (48) Esteban, G.; López-Sánchez, M. A.; Martínez, M.; Plumet, J. *Tetrahedron* **1998**, *54*, 197.
- (49) Bordwell, F. G. *Acc. Chem. Res.* **1988**, *21*, 456

